

X-rays constraints on sub-GeV dark matter

Based on work with M. Cirelli, N. Fornengo, E. Pinetti & B. M. Roach

JCAP 07 (2023) 026 [arXiv:2303.08854]

Jordan Koechler

LPTHE, Sorbonne University, Paris

TeVPA 2023



Introduction

Introduction

- Null results on WIMPs in colliders, direct and indirect detection

Introduction

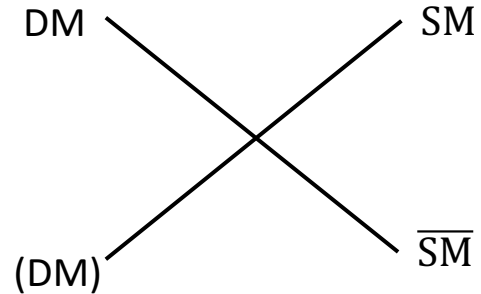
- Null results on WIMPs in colliders, direct and indirect detection
- A lot of ‘light’ DM models are well-motivated:
 - Hidden sector/secluded DM
 - SIMP DM
 - Asymmetric DM
 - ...

Introduction

- Null results on WIMPs in colliders, direct and indirect detection
- A lot of ‘light’ DM models are well-motivated:
 - Hidden sector/secluded DM
 - SIMP DM
 - Asymmetric DM
 - ...
- Light DM detection is challenging

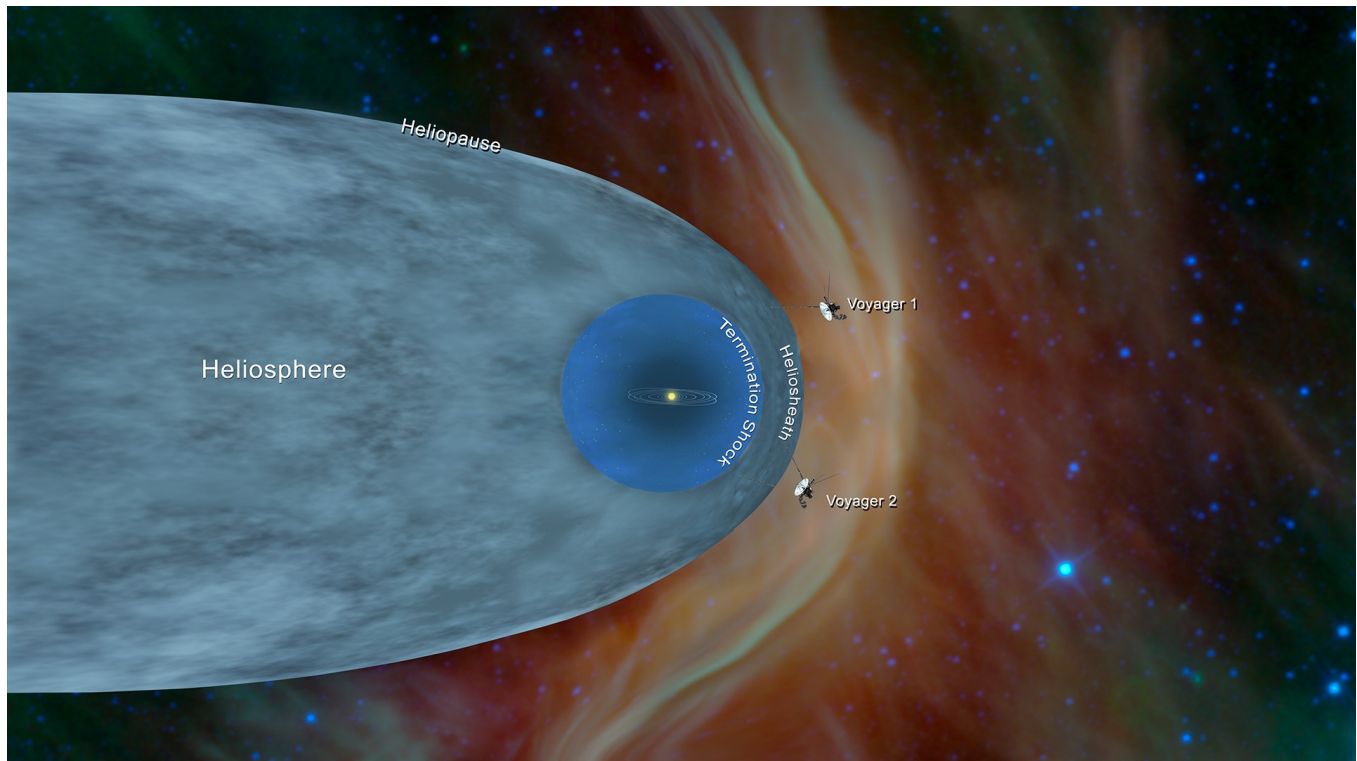
Introduction

Indirect detection
→



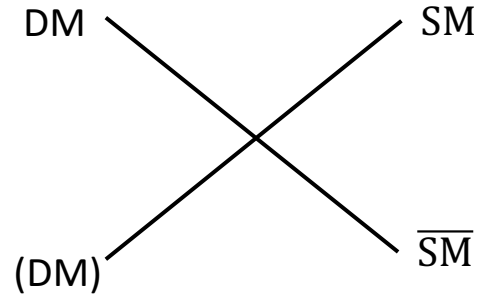
Issue in Indirect Detection:

Solar winds are a barrier to low-energy charged particles



Introduction

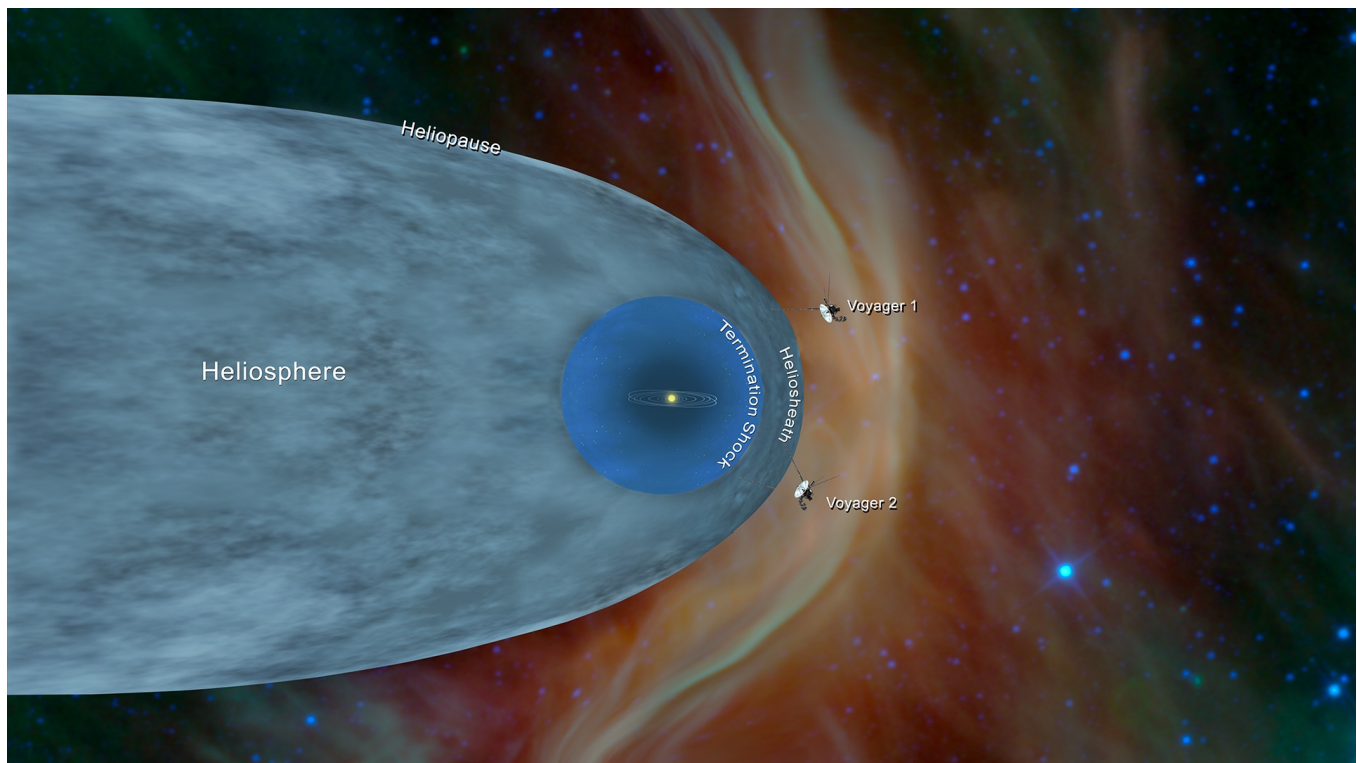
Indirect detection
→

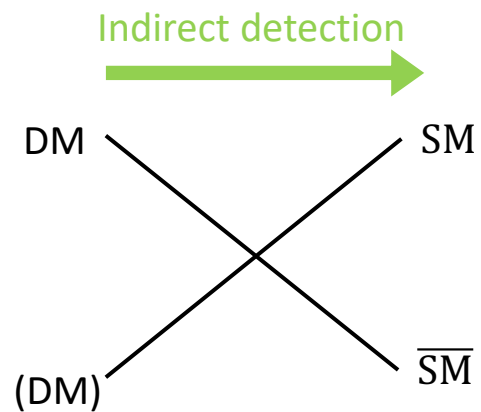


Issue in Indirect Detection:

Solar winds are a barrier to low-energy charged particles

Solutions:





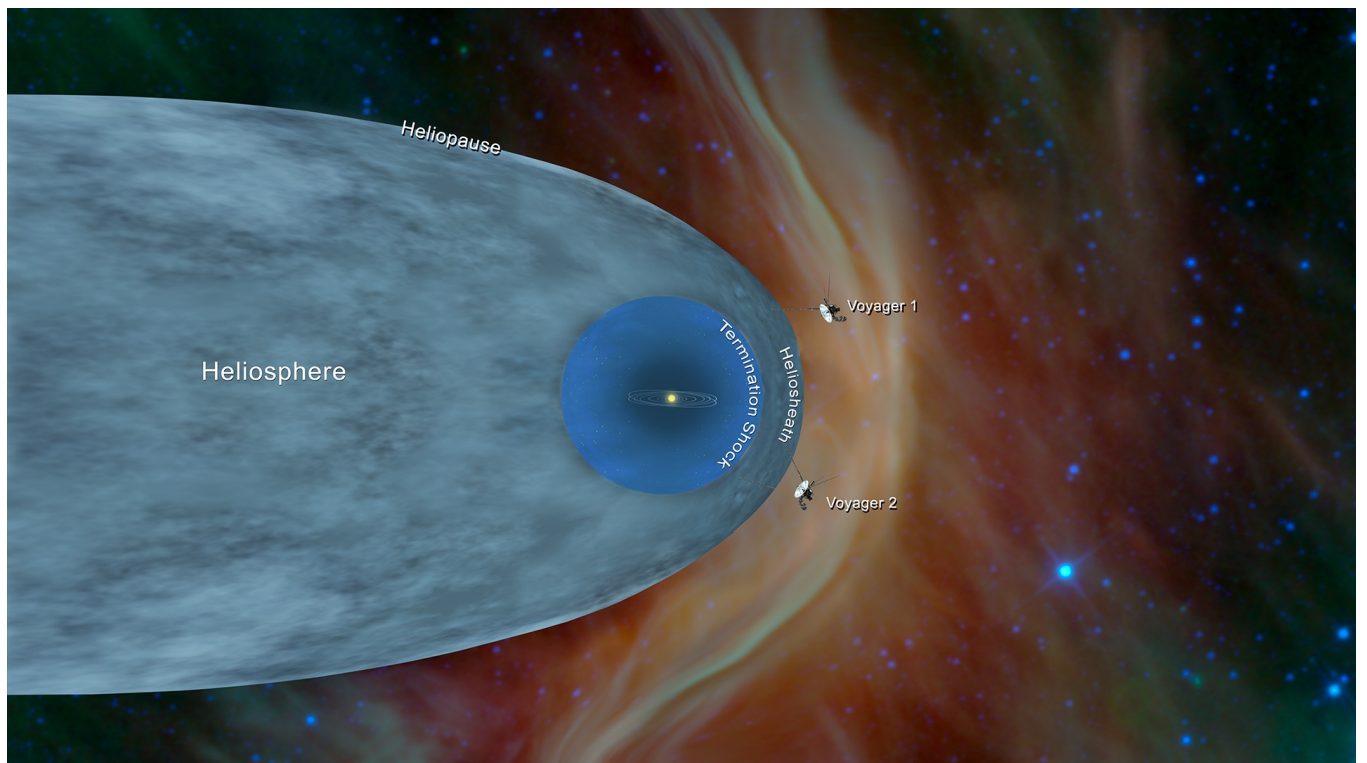
Introduction

Issue in Indirect Detection:

Solar winds are a barrier to low-energy charged particles

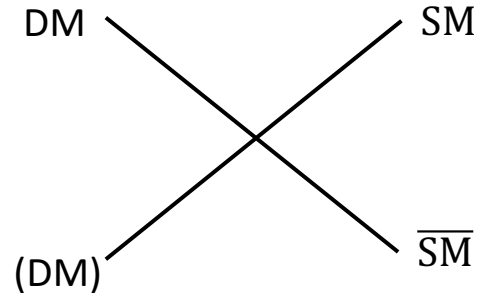
Solutions:

- Look at Voyager1 & 2 data!



Introduction

Indirect detection
→

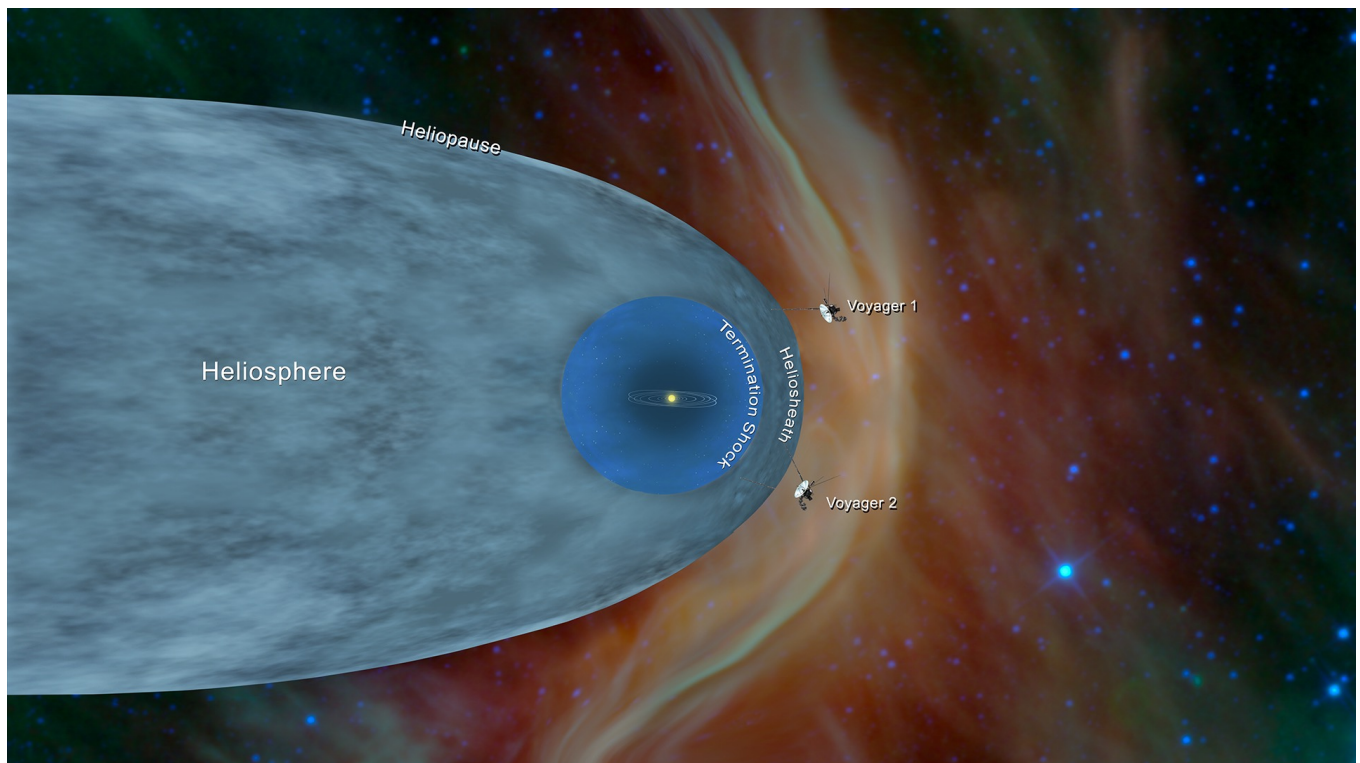


Issue in Indirect Detection:

Solar winds are a barrier to low-energy charged particles

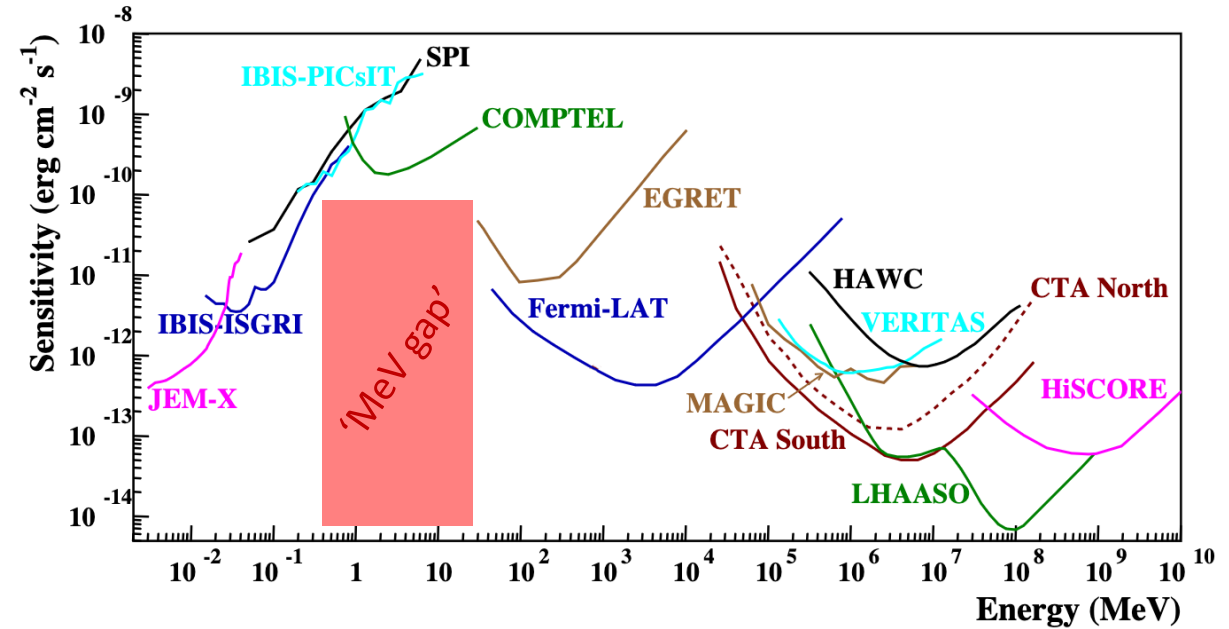
Solutions:

- Look at Voyager1 & 2 data!
- What about photons?



Introduction

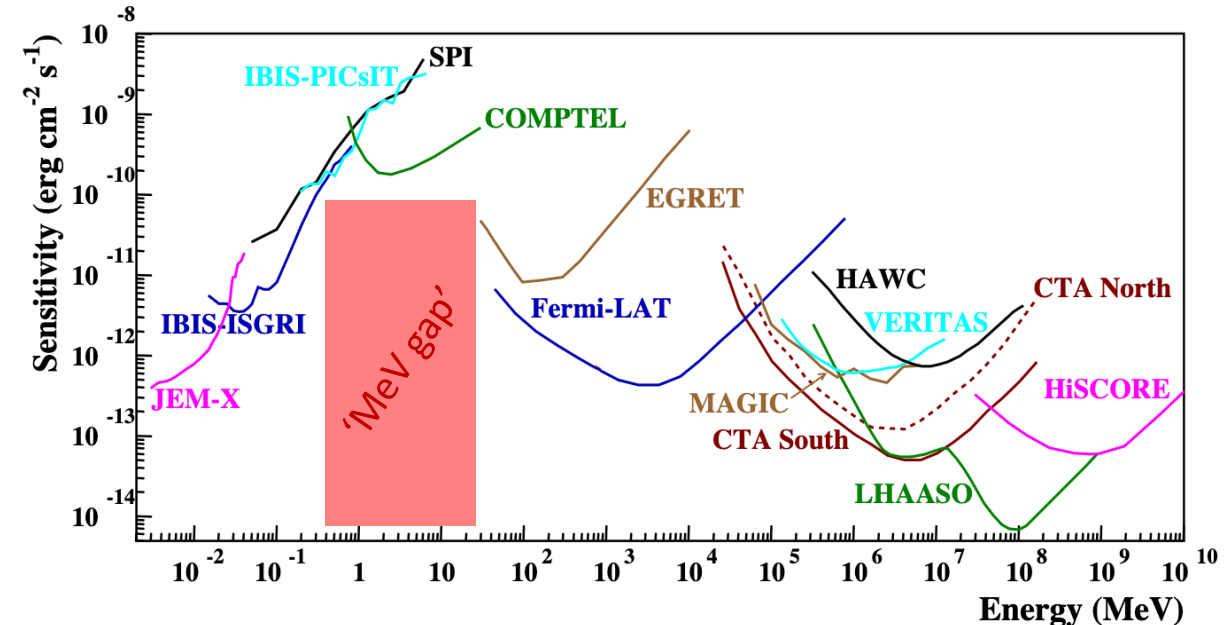
- No data of quality for γ -rays between $\sim 100 \text{ keV} - 100 \text{ MeV}$



Adapted from [De Angelis et al., AMEGO coll., 1611.02232](#)

Introduction

- No data of quality for γ -rays between $\sim 100 \text{ keV} - 100 \text{ MeV}$
- We focus on secondary emissions to circumvent this problem, and study light DM signals in the Milky Way using X-rays



Adapted from [De Angelis et al., AMEGO coll., 1611.02232](#)

X-rays from DM
annihilation/decay

X-rays from DM annihilation/decay

- There are a few ways to generate X-rays from DM annihilation/decay :

X-rays from DM annihilation/decay

- There are a few ways to generate X-rays from DM annihilation/decay :
 - Prompt emissions:
 - Secondary emissions (energy loss):

X-rays from DM annihilation/decay

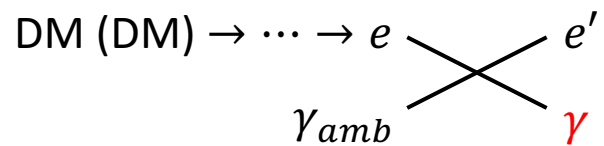
- There are a few ways to generate X-rays from DM annihilation/decay :
 - Prompt emissions:
 - **Final state radiation (FSR):** DM (DM) $\rightarrow \mu^+ \mu^- \gamma$
 - Secondary emissions (energy loss):

X-rays from DM annihilation/decay

- There are a few ways to generate X-rays from DM annihilation/decay :
 - Prompt emissions:
 - **Final state radiation (FSR)**: $\text{DM} (\text{DM}) \rightarrow \mu^+ \mu^- \gamma$
 - **Radiative decay (Rad)**: $\text{DM} (\text{DM}) \rightarrow \mu^+ \mu^- \rightarrow \mu^+ e^- \bar{\nu}_e \nu_\mu \gamma$
 - Secondary emissions (energy loss):

X-rays from DM annihilation/decay

- There are a few ways to generate X-rays from DM annihilation/decay :
 - Prompt emissions:
 - **Final state radiation (FSR)**: $\text{DM} \rightarrow \mu^+ \mu^- \gamma$
 - **Radiative decay (Rad)**: $\text{DM} \rightarrow \mu^+ \mu^- \rightarrow \mu^+ e^- \bar{\nu}_e \nu_\mu \gamma$
 - Secondary emissions (energy loss):
 - **Inverse-Compton scattering**: up-scattering of ambient photons thanks to DM-produced e^\pm



X-rays from DM annihilation/decay

- We consider the following mass range for DM:

$$1 \text{ MeV} < m_{DM} < 5 \text{ GeV}$$

X-rays from DM annihilation/decay

- We consider the following mass range for DM:

$$1 \text{ MeV} < m_{DM} < 5 \text{ GeV}$$

- Kinematically open primary channels that produce e^\pm one way or another:

X-rays from DM annihilation/decay

- We consider the following mass range for DM:

$$1 \text{ MeV} < m_{DM} < 5 \text{ GeV}$$

- Kinematically open primary channels that produce e^\pm one way or another:
 - DM (DM) $\rightarrow e^+e^-$

X-rays from DM annihilation/decay

- We consider the following mass range for DM:

$$1 \text{ MeV} < m_{DM} < 5 \text{ GeV}$$

- Kinematically open primary channels that produce e^\pm one way or another:
 - DM (DM) $\rightarrow e^+e^-$
 - DM (DM) $\rightarrow \mu^+\mu^-$ ($\mu^\pm \rightarrow e^\pm \nu_e \nu_\mu$ @ $\sim 100\%$)

X-rays from DM annihilation/decay

- We consider the following mass range for DM:

$$1 \text{ MeV} < m_{DM} < 5 \text{ GeV}$$

- Kinematically open primary channels that produce e^\pm one way or another:
 - DM (DM) $\rightarrow e^+e^-$
 - DM (DM) $\rightarrow \mu^+\mu^-$ ($\mu^\pm \rightarrow e^\pm\nu_e\nu_\mu$ @ $\sim 100\%$)
 - DM (DM) $\rightarrow \pi^+\pi^-$ ($\pi^\pm \rightarrow \mu^\pm\nu_\mu$ @ $\sim 100\%$)

X-rays from DM annihilation/decay

- Differential flux of photons from prompt emissions:

X-rays from DM annihilation/decay

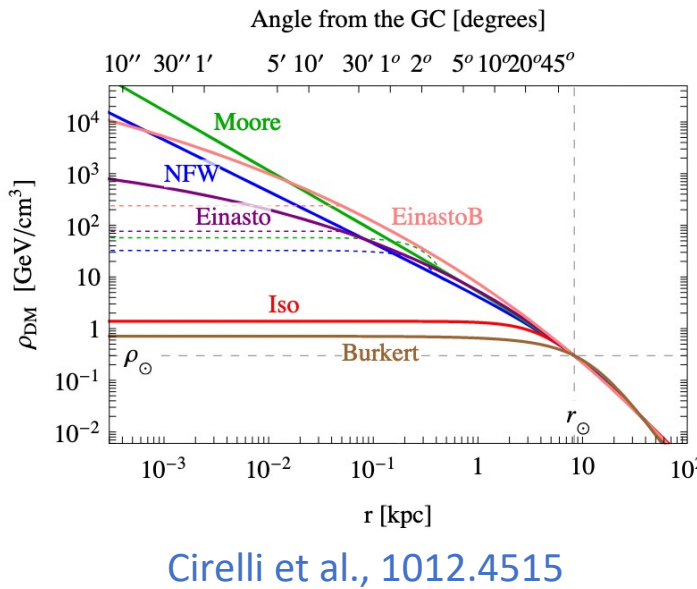
- Differential flux of photons from prompt emissions:

$$f = \text{FSR, Rad} \quad \frac{d\Phi_{f,\gamma}}{dE_\gamma d\Omega} = \frac{1}{4\pi} \frac{dN_\gamma^f}{dE_\gamma} \times \begin{cases} \frac{1}{2} \frac{\langle \sigma v \rangle}{m_{DM}^2} \int_{l.o.s.} \rho_{DM}^2 ds & \text{(annihilation)} \\ \frac{\Gamma}{m_{DM}} \int_{l.o.s.} \rho_{DM} ds & \text{(decay)} \end{cases}$$

X-rays from DM annihilation/decay

- Differential flux of photons from prompt emissions:

$$f = \text{FSR, Rad} \quad \frac{d\Phi_{f,\gamma}}{dE_\gamma d\Omega} = \frac{1}{4\pi} \frac{dN_\gamma^f}{dE_\gamma} \times \begin{cases} \frac{1}{2} \frac{\langle \sigma v \rangle}{m_{DM}^2} \int_{l.o.s.} \rho_{DM}^2 ds \\ \frac{\Gamma}{m_{DM}} \int_{l.o.s.} \rho_{DM} ds \end{cases}$$

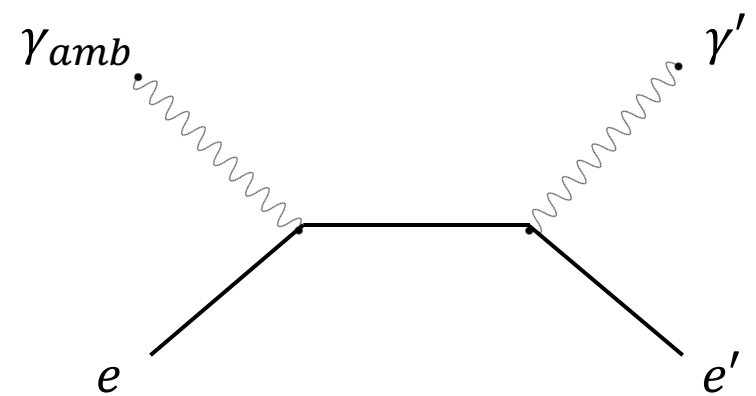


(annihilation)

(decay)

X-rays from DM annihilation/decay

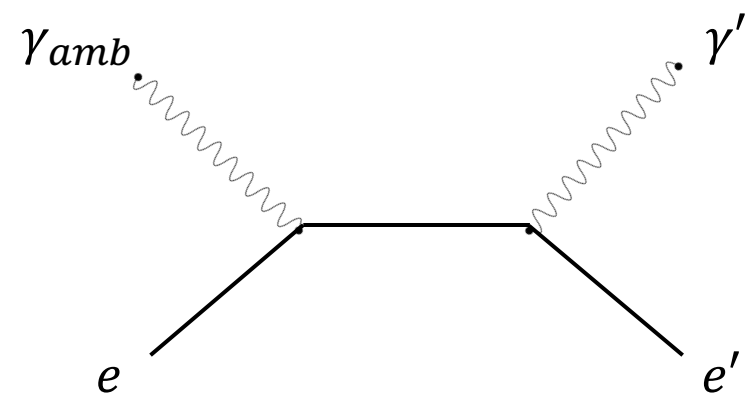
- DM-produced e^\pm can up-scatter ambient photons up to X-ray energies



$$E_{\gamma'} \approx 4\gamma_e^2 E_{\gamma_{amb}} \quad \gamma_e = \frac{E_e}{m_e}$$

X-rays from DM annihilation/decay

- DM-produced e^\pm can up-scatter ambient photons up to X-ray energies



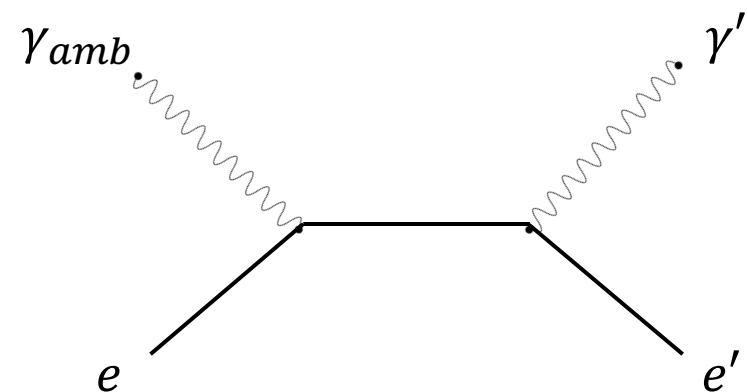
$$E_{\gamma'} \approx 4\gamma_e^2 E_{\gamma_{amb}} \quad \gamma_e = \frac{E_e}{m_e}$$

For a CMB photon up-scattered by a 1 GeV e^\pm :
 $E_{\gamma_{amb}} \approx 0.2 \text{ meV} \rightarrow E_{\gamma'} \approx 3 \text{ keV}$

- Ambient photons are: **CMB, dust-rescattered IR and optical starlight (SL)**
- Energy range $\sim 0.1 \text{ meV}$ to 10 eV

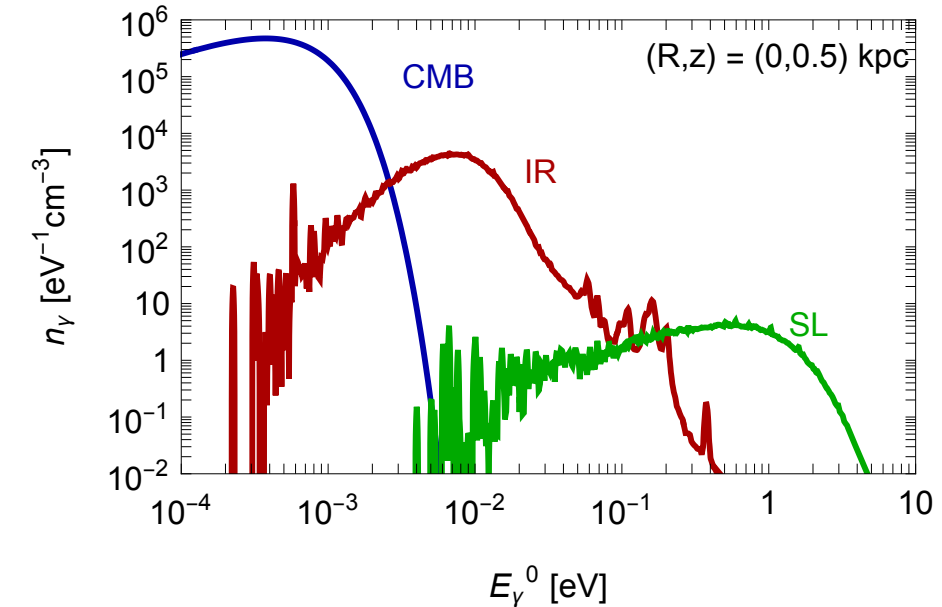
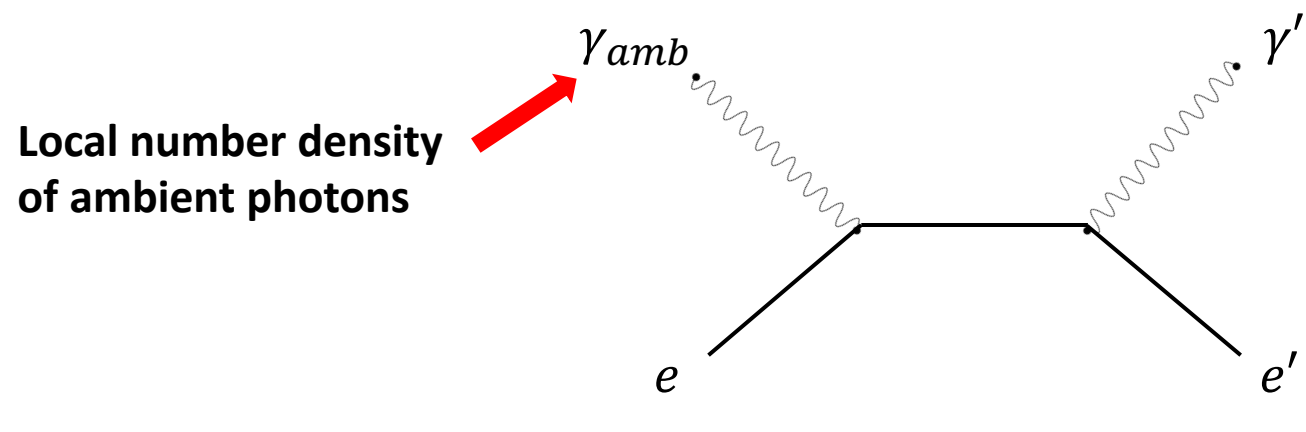
X-rays from DM annihilation/decay

- To compute the IC-scattered photon flux, we need a few ingredients:



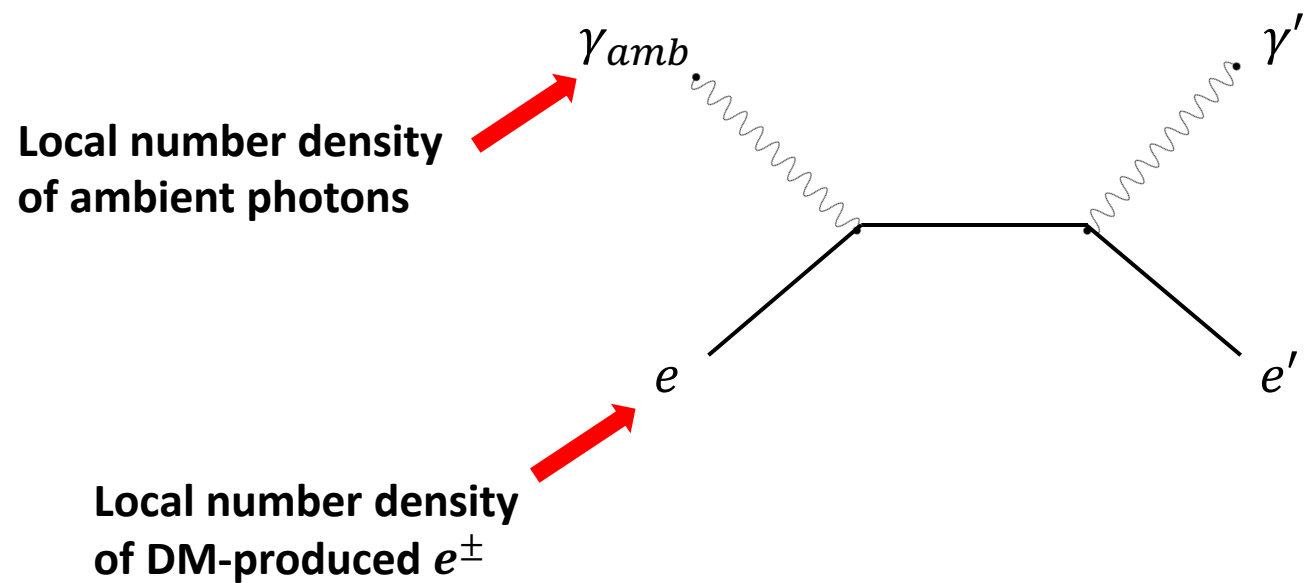
X-rays from DM annihilation/decay

- To compute the IC-scattered photon flux, we need a few ingredients:



X-rays from DM annihilation/decay

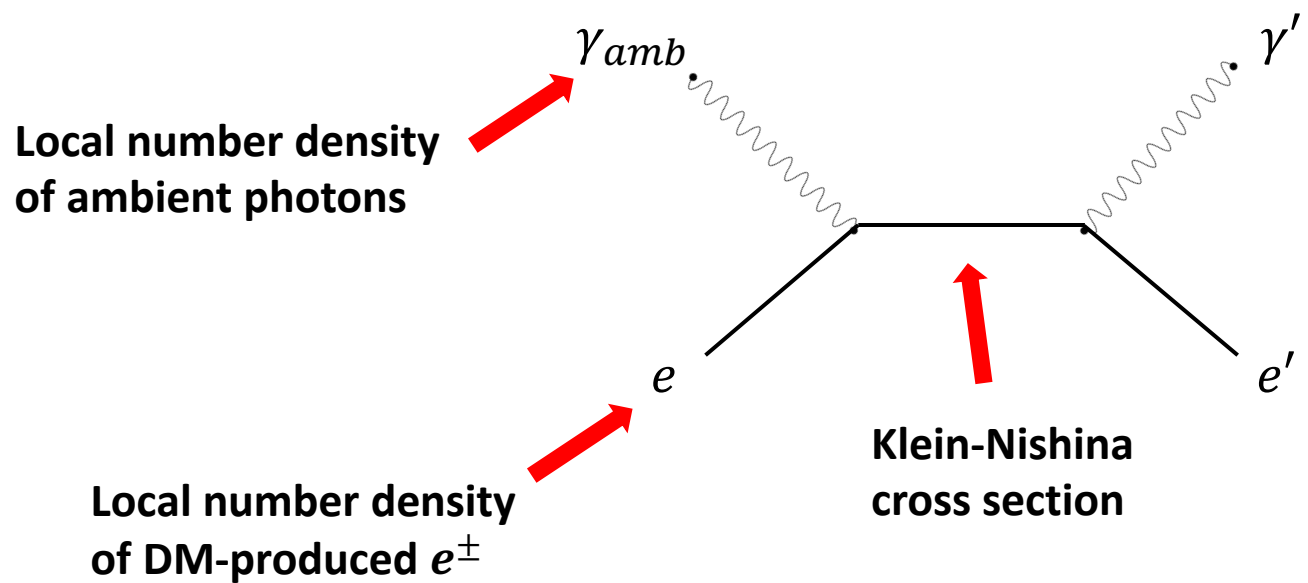
- To compute the IC-scattered photon flux, we need a few ingredients:



$$\frac{\partial f}{\partial t} = \nabla(\mathcal{K}(E_e, \vec{x}) \nabla f) + \frac{\partial}{\partial E_e} (b(E_e, \vec{x}) f) + Q(E_e, \vec{x})$$

X-rays from DM annihilation/decay

- To compute the IC-scattered photon flux, we need a few ingredients:

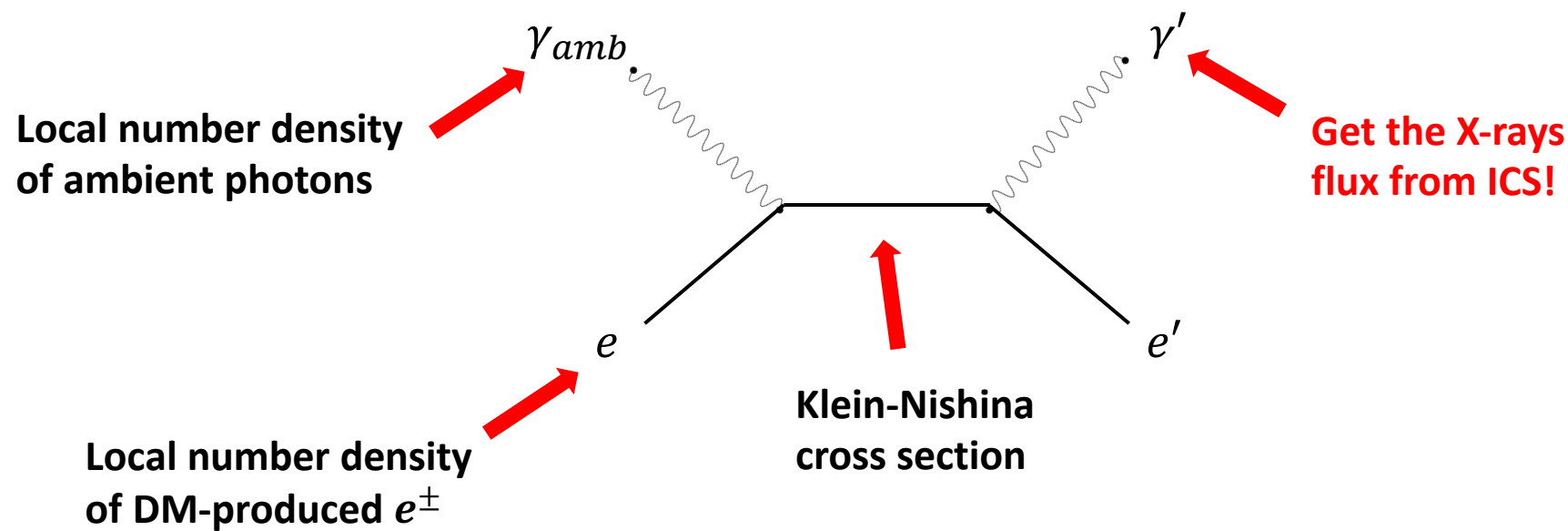


$$\sigma_{IC}(y, E_e) = \frac{3\sigma_T}{4\gamma_e^2} \frac{2y \ln y + y + 1 - 2y^2}{y}$$

$$y = \frac{E_\gamma}{4\gamma_e^2 E_\gamma^0}, \quad \gamma_e = \frac{E_e}{m_e}$$

X-rays from DM annihilation/decay

- To compute the IC-scattered photon flux, we need a few ingredients:



Analysis and results

Analysis and results

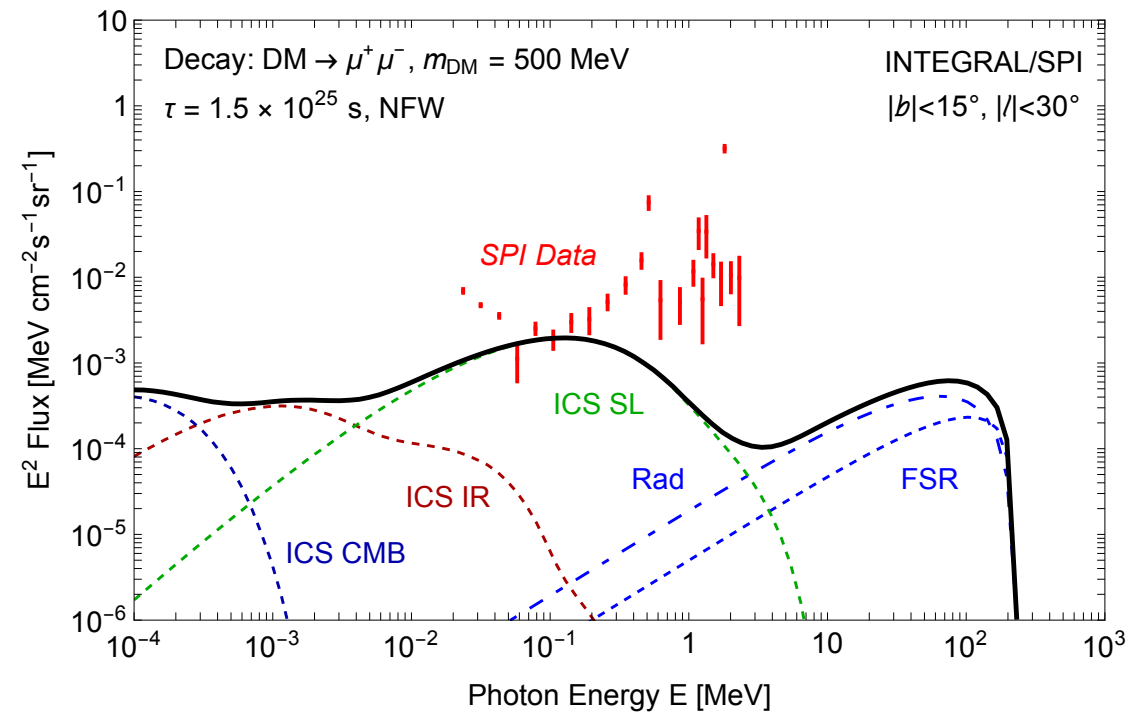
- In this study we keep a **conservative** approach:

Analysis and results

- In this study we keep a **conservative** approach:

$$\chi^2(p, m_{DM}) = \sum_{i \in \text{bins}} \frac{\text{Max}(\Phi_{DM\gamma,i}(p, m_{DM}) - \Phi_i, 0)^2}{\sigma_i^2}$$

$$p = \langle \sigma v \rangle, \Gamma$$



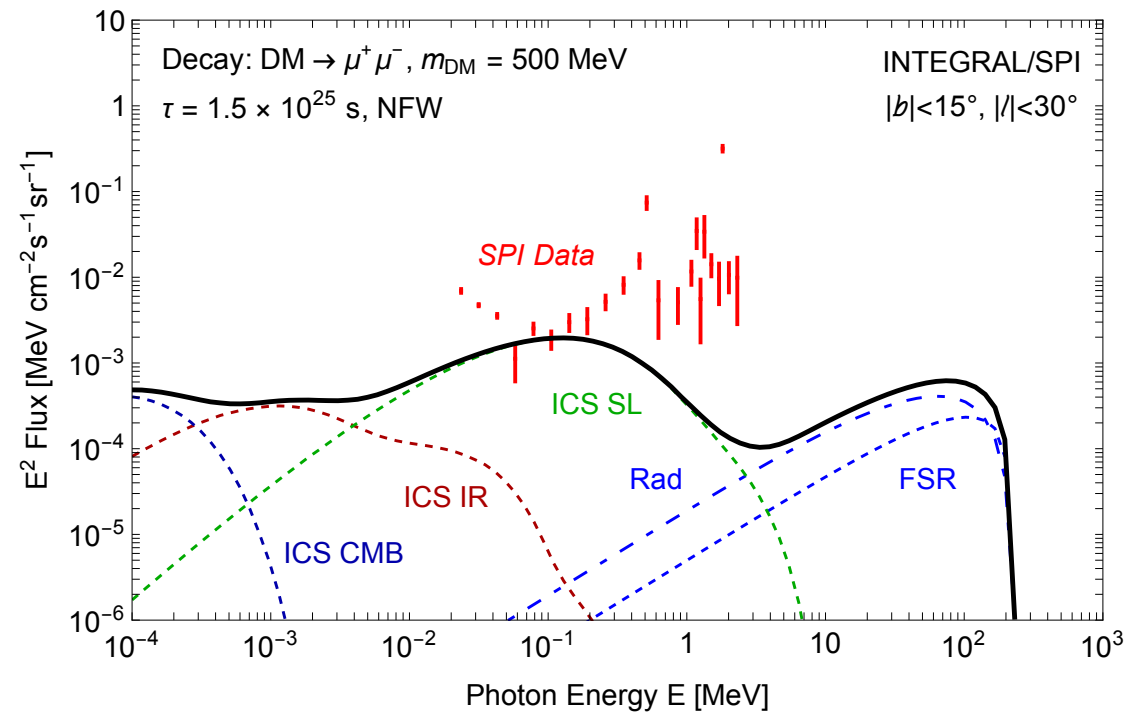
Analysis and results

- In this study we keep a **conservative** approach:

$$\chi^2_{>}(\mathbf{p}, m_{DM}) = \sum_{i \in \text{bins}} \frac{\text{Max}(\Phi_{DM\gamma,i}(\mathbf{p}, m_{DM}) - \Phi_i, 0)^2}{\sigma_i^2}$$

$$\mathbf{p} = \langle \sigma v \rangle, \Gamma$$

- Impose a bound when $\chi^2_{>}(\mathbf{p}, m_{DM}) \geq 4$



Analysis and results

INTEGRAL diffuse emission searches

2003-2009

Bouchet et al., INTEGRAL coll., 1107.0200

NuSTAR
2012-2018

Blank-sky fields

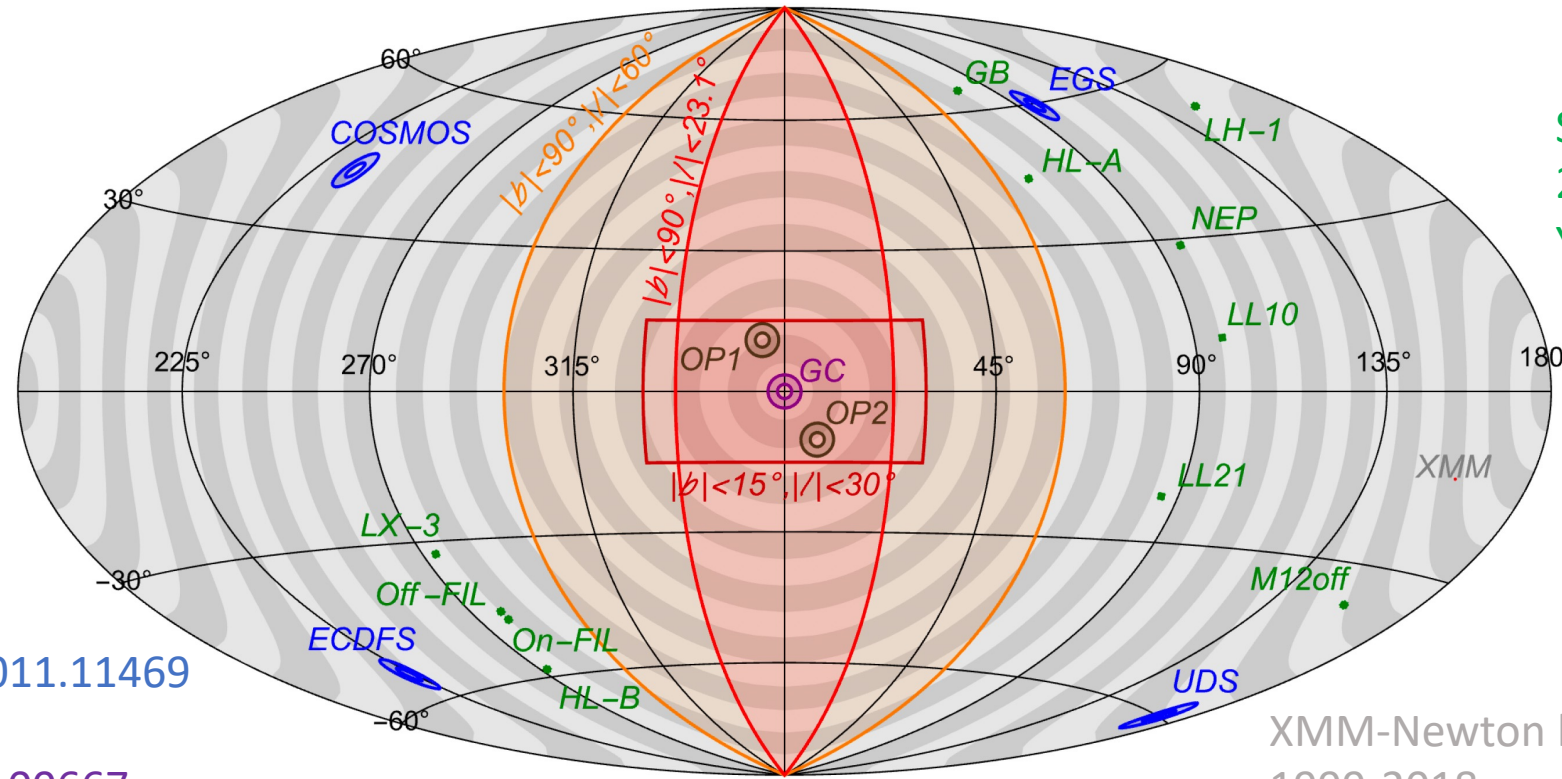
Krionos et al., 2011.11469

GC observations

Perez et al., 1609.00667

Off-plane observations

Roach et al., 1908.09037



Suzaku high-latitude fields
2006-2008
Yoshino et al., 0903.2981

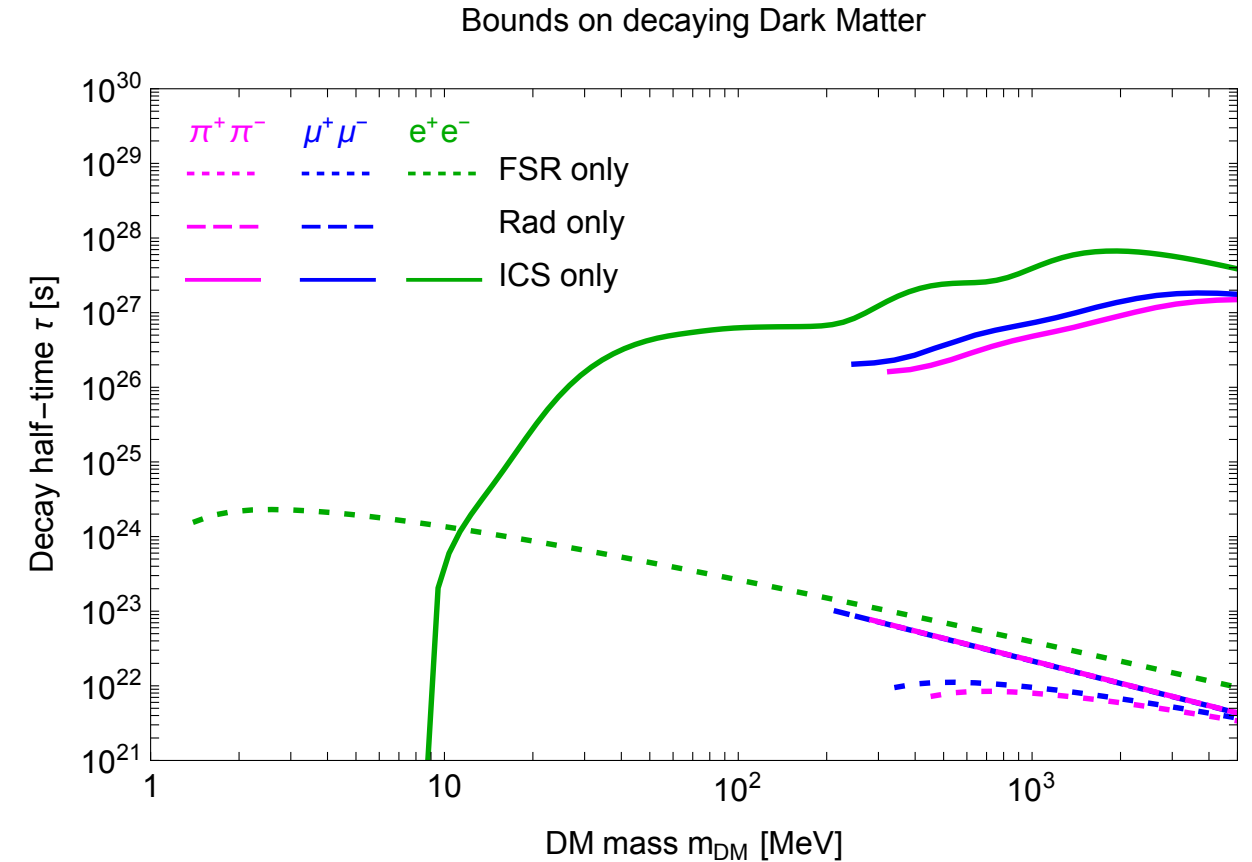
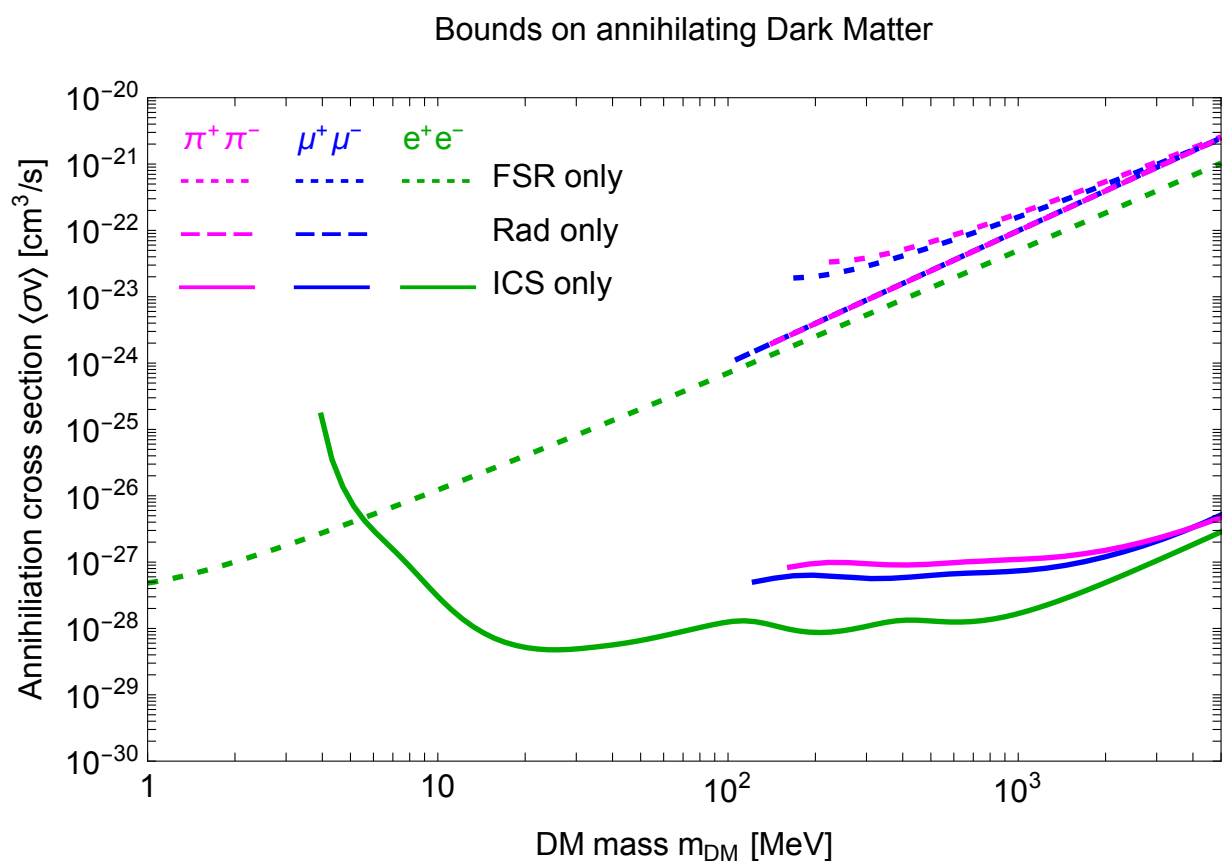
XMM-Newton blank-sky data

1999-2018

Foster et al., 2102.02207

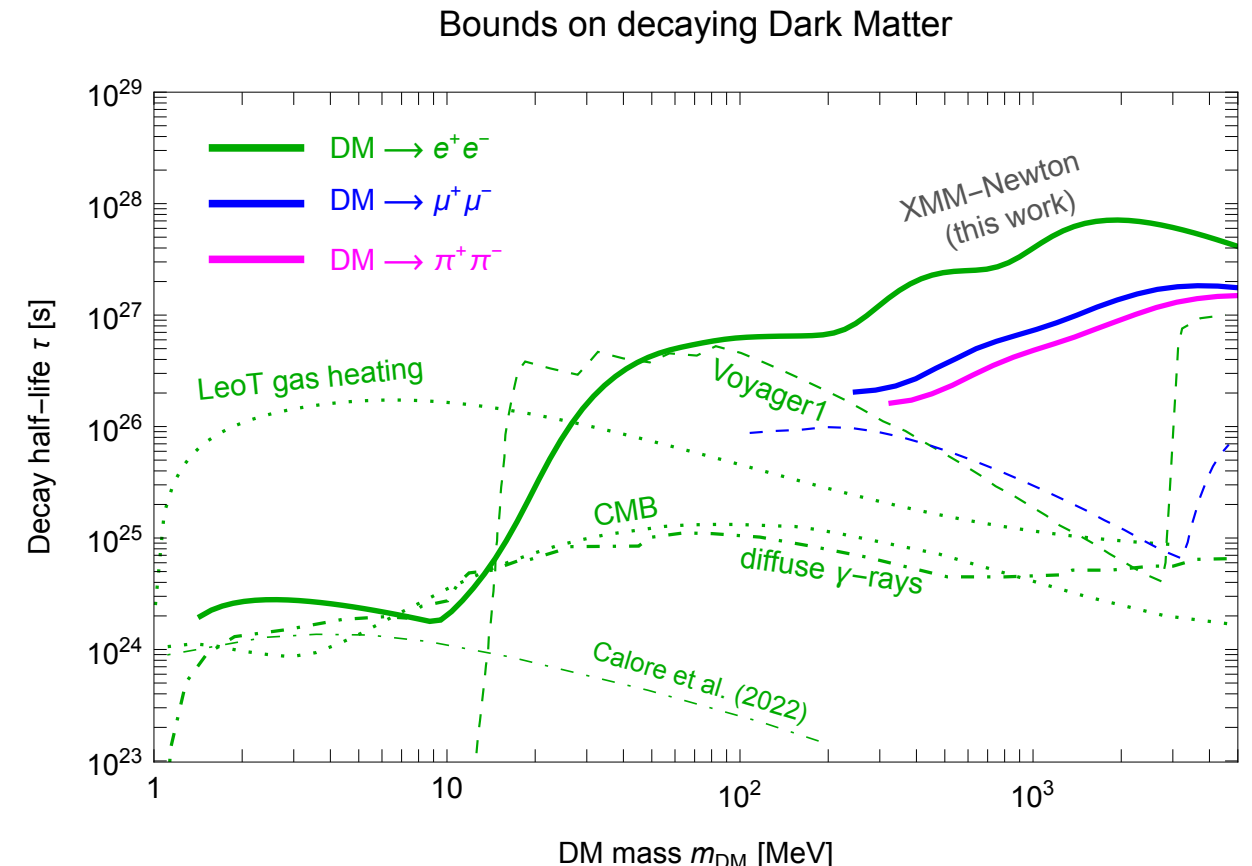
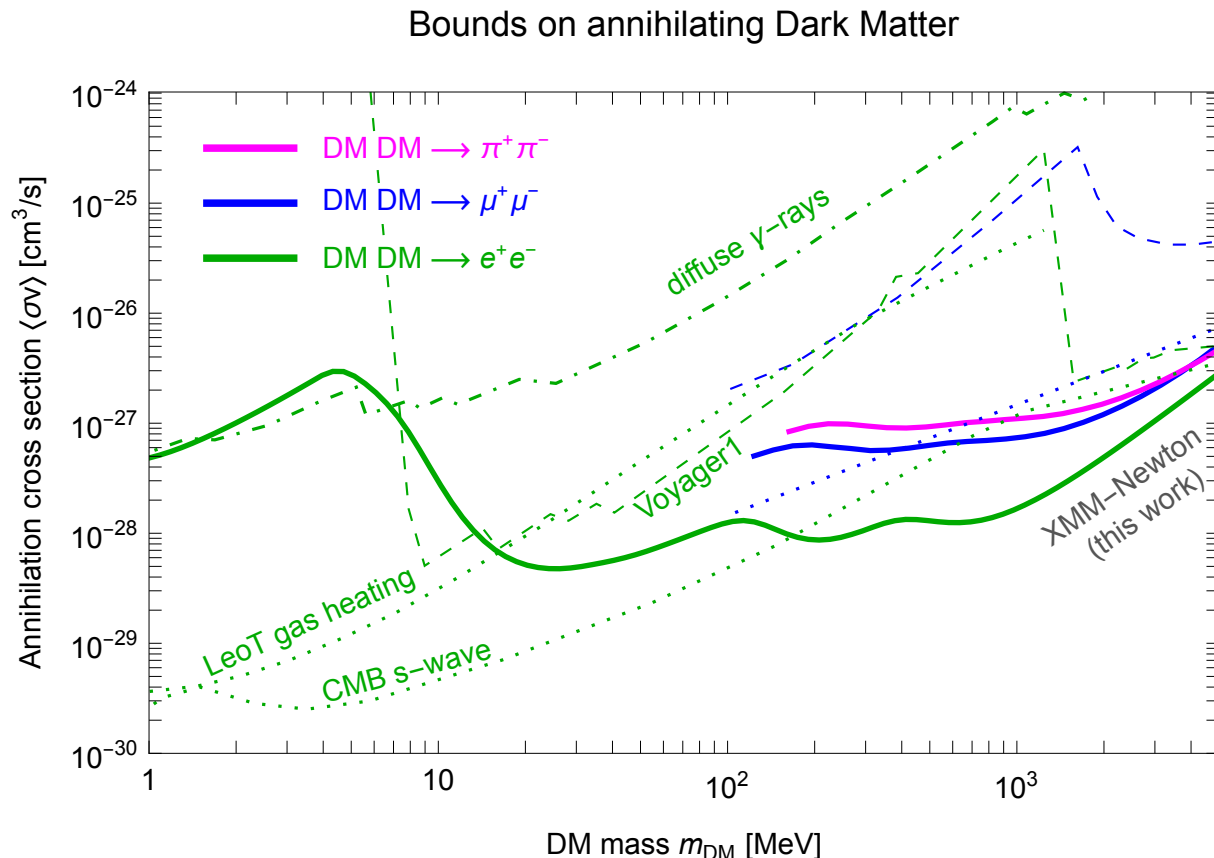
https://github.com/bsafdi/XMM_BSO_DATA

Analysis and results

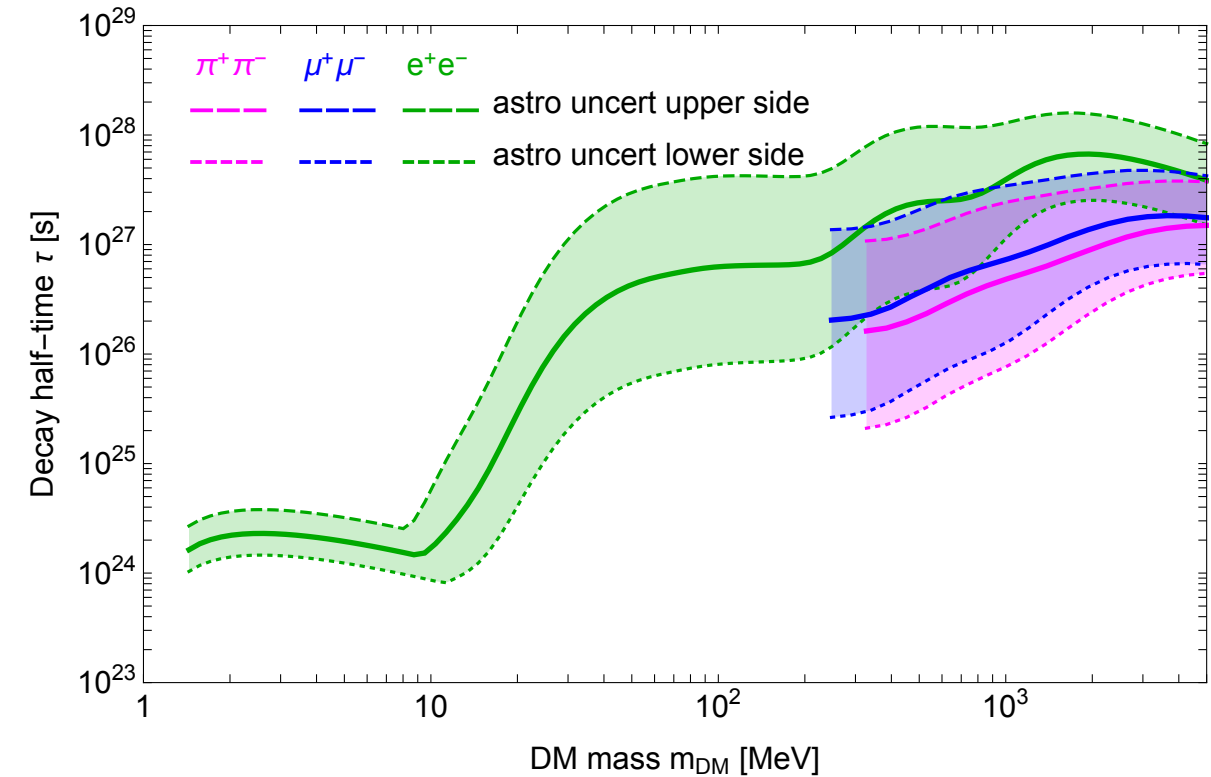
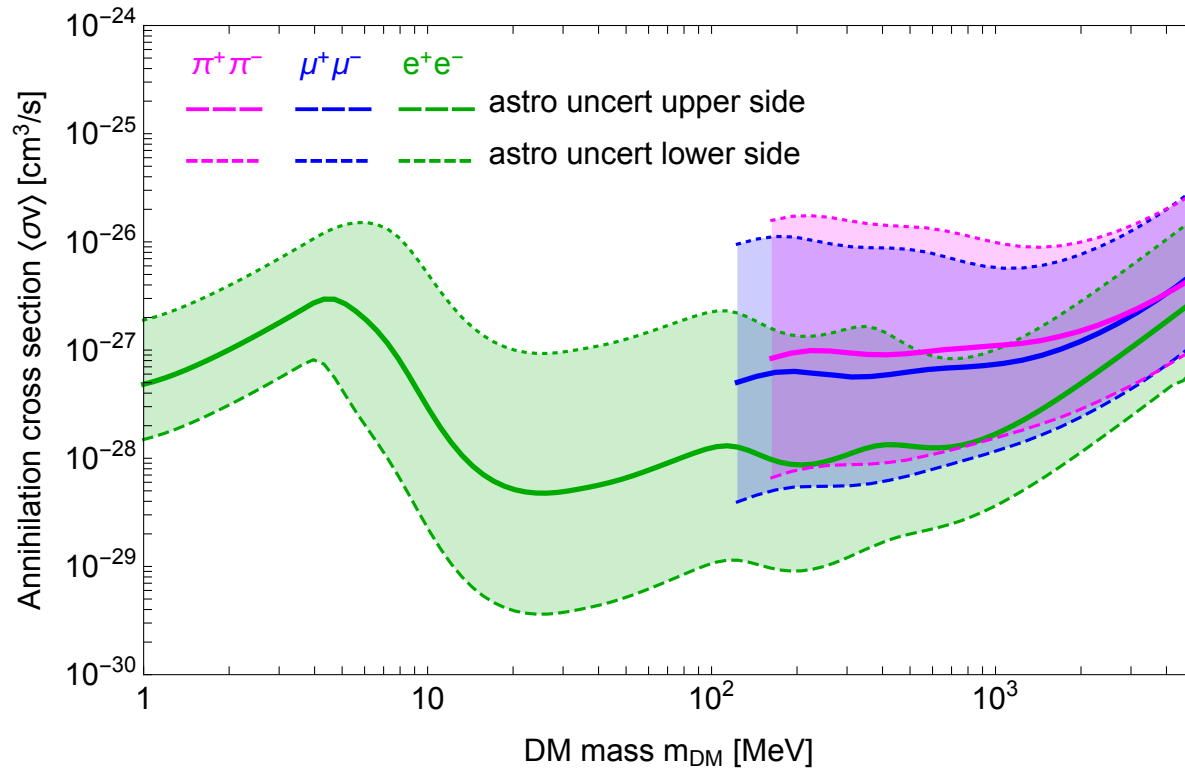


Analysis and results

Diffuse γ -rays: [Essig et al., 1309.4091](#)
 Voyager1: [Boudaud et al., 1612.07698](#)
 Leo T gas heating: [Wakedar and Wang, 2111.08025](#)
 CMB (s-wave): [Slatyer, 1506.03811](#),
[Lopez-Honorez et al., 1303.5094](#),
[Liu et al., 1604.02457](#)
 INTEGRAL FSR: [Calore et al. 2209.06299](#)



Analysis and results



Summary

Summary

- Using secondary emission flux computations, we can compute strong bounds on light DM, while circumventing the MeV gap

Summary

- Using secondary emission flux computations, we can compute strong bounds on light DM, while circumventing the MeV gap
- Background modeling?

Summary

- Using secondary emission flux computations, we can compute strong bounds on light DM, while circumventing the MeV gap
- Background modeling?
- Other possible directions: p-wave annihilation, consider DM annihilation/decay channels in exotic resonances, ...

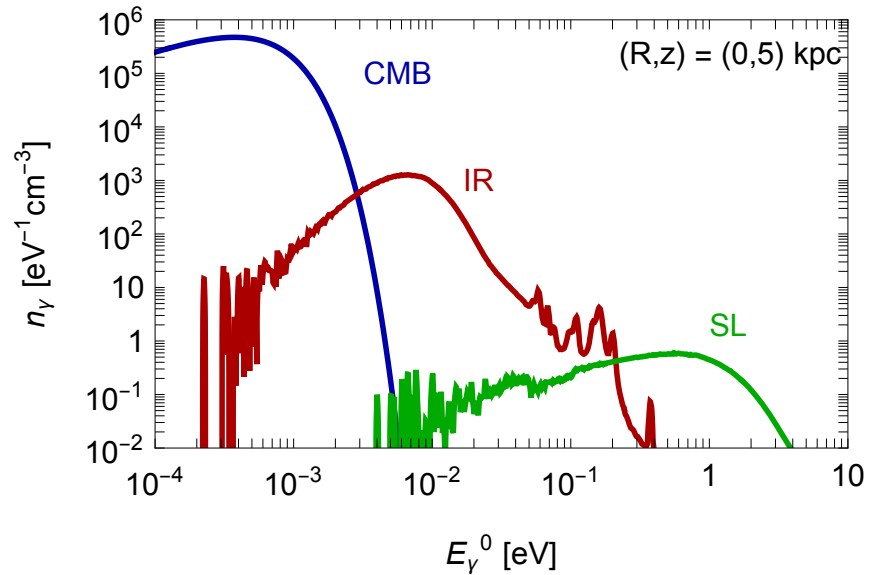
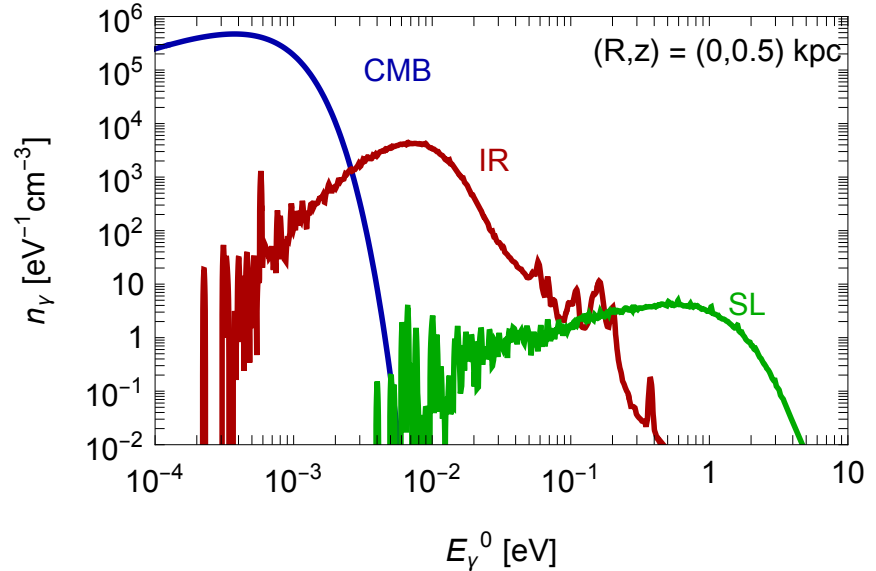
Thank you for your attention!

Backup

Inverse-Compton scattering

1) Local number density of ISRF photons:

- For CMB, we derive using Planck's law
- For IR and SL, we use GalPROP intensity maps, in turn based on actual observations from COBE/DIRBE



Inverse-Compton scattering

2) Local number density of DM produced e^\pm :

$$\cancel{\frac{\partial f}{\partial t}} = \cancel{\nabla(\mathcal{R}(E_e, \vec{x}) \nabla f)} + \frac{\partial}{\partial E_e} (b(E_e, \vec{x}) f) + Q(E_e, \vec{x})$$

diffusion term

energy loss term

source term

- We study the stationary regime
- For high-energy e^\pm in the Milky Way, energy loss dominate over diffusion

Inverse-Compton scattering

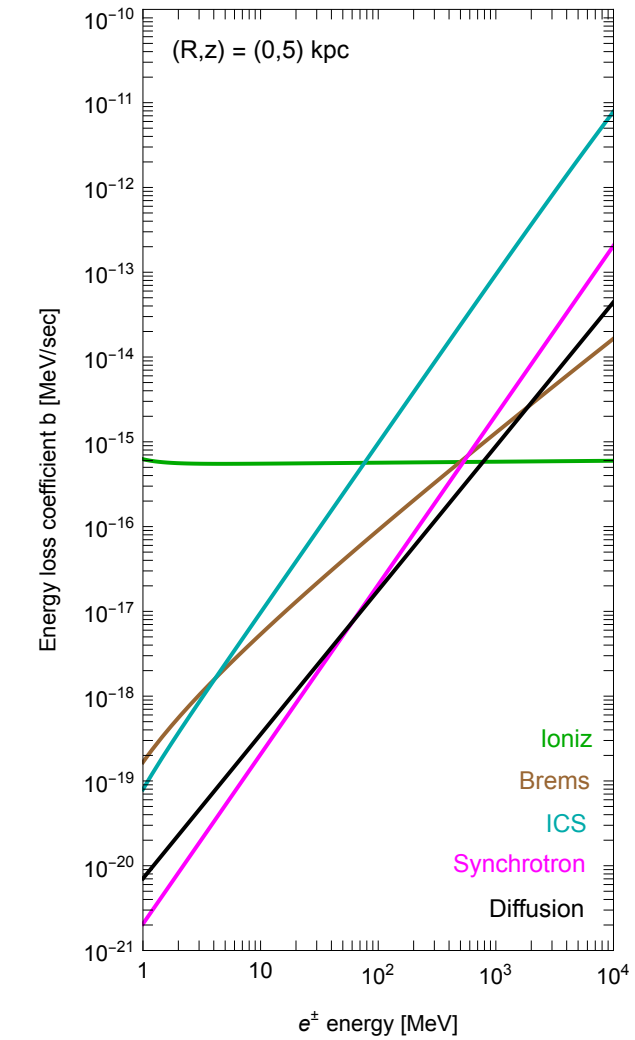
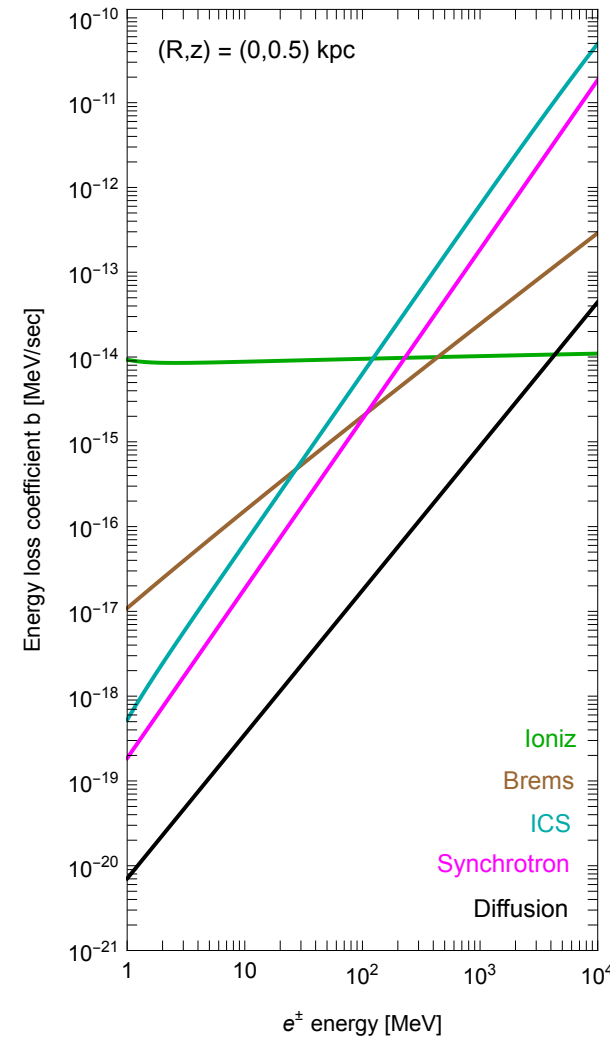
$$b(E_e, \vec{x}) = b_{Coul+ioniz} + b_{brems} + b_{ICS} + b_{syn}$$

Depends on the local ISRF density

Depend on the local gas density

Depends on the galactic magnetic field configuration

- $b(E_e, \vec{x})$ taken from [PPPC4DMID](#)
- Diffusion curve: $b_{diff}(E_e) \sim E_e / \tau_{diff}(E_e)$



Inverse-Compton scattering

- Source term:
$$Q(E_e, \vec{x}) = \begin{cases} \frac{\langle \sigma v \rangle}{2} \left(\frac{\rho_{DM}(\vec{x})}{m_{DM}} \right)^2 \frac{dN_{e^\pm}}{dE_e} \\ \Gamma \left(\frac{\rho_{DM}(\vec{x})}{m_{DM}} \right) \frac{dN_{e^\pm}}{dE_e} \end{cases}$$
- Where $\frac{dN_{e^\pm}}{dE_e}$ is the e^\pm injection spectrum:
 - For the $e^+ e^-$ channel: monochromatic ($DM \rightarrow e^\pm$)
 - For the $\mu^+ \mu^-$ channel: boosted Michel spectrum ($DM \rightarrow \mu^\pm \rightarrow e^\pm$)
 - For the $\pi^+ \pi^-$ channel: double boosted Michel spectrum ($DM \rightarrow \pi^\pm \rightarrow \mu^\pm \rightarrow e^\pm$)

Michel spectrum and boosts

- Michel spectrum: $\frac{dN_e^{\mu \rightarrow e\nu\bar{\nu}}}{dE_e} = \frac{4\sqrt{\xi^2 - 4\varrho^2}}{m_\mu} [\xi(3 - 2\xi) + \varrho^2(3\xi - 4)]$

$$\xi = \frac{2E_e}{m_\mu}, \quad \varrho = \frac{m_e}{m_\mu}$$

- Lorentz boost: $\frac{dN}{dE} = \frac{1}{2\beta\gamma} \int_{E'_{min}}^{E'_{max}} \frac{1}{p'} \frac{dN}{dE'}$ $E'_{\max|min} = \gamma(E \pm \beta p)$

$$\gamma = \frac{E_A}{m_A} \quad (\text{A} = \text{parent particle})$$

Inverse-Compton scattering

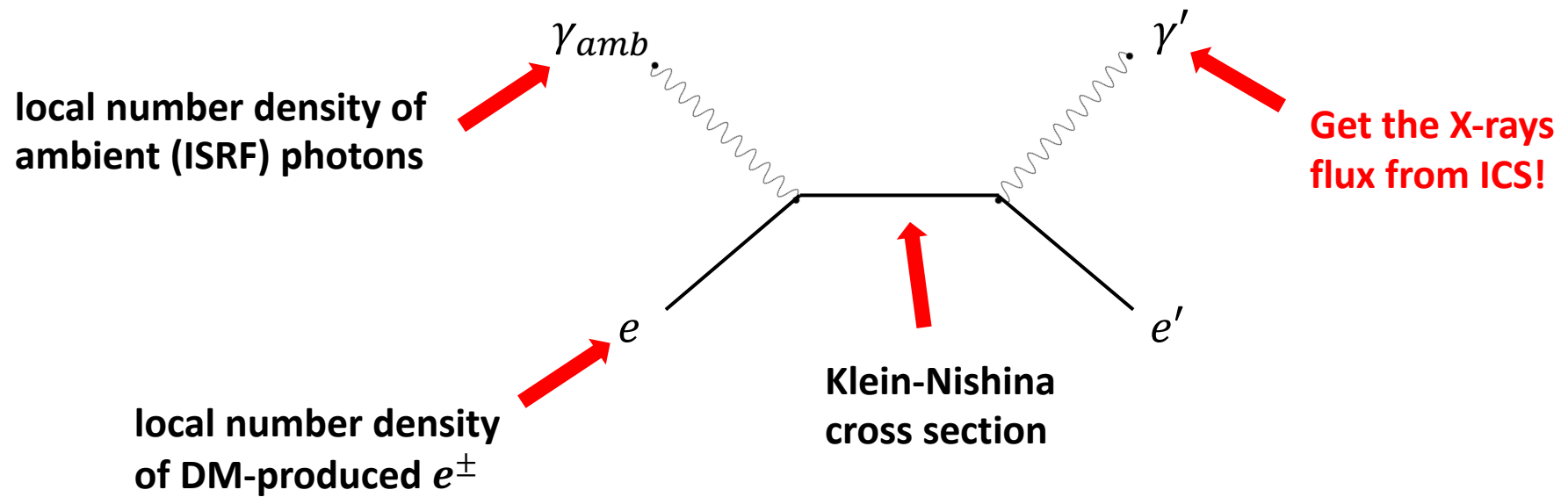
3) Klein-Nishina cross section (in the Thomson limit: $E_\gamma^0 \ll E_e$)

$$\sigma_{IC}(y, E_e) = \frac{3\sigma_T}{4\gamma_e^2} \frac{2y \ln y + y + 1 - 2y^2}{y}$$

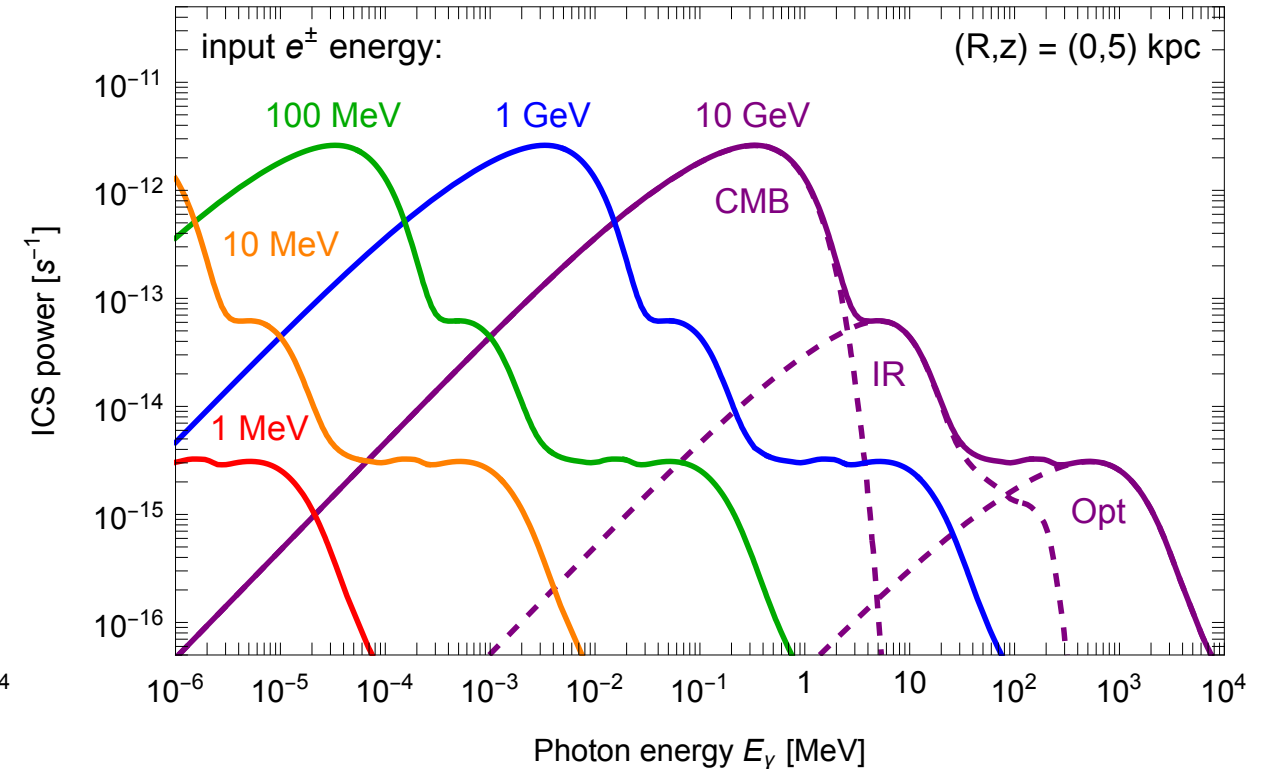
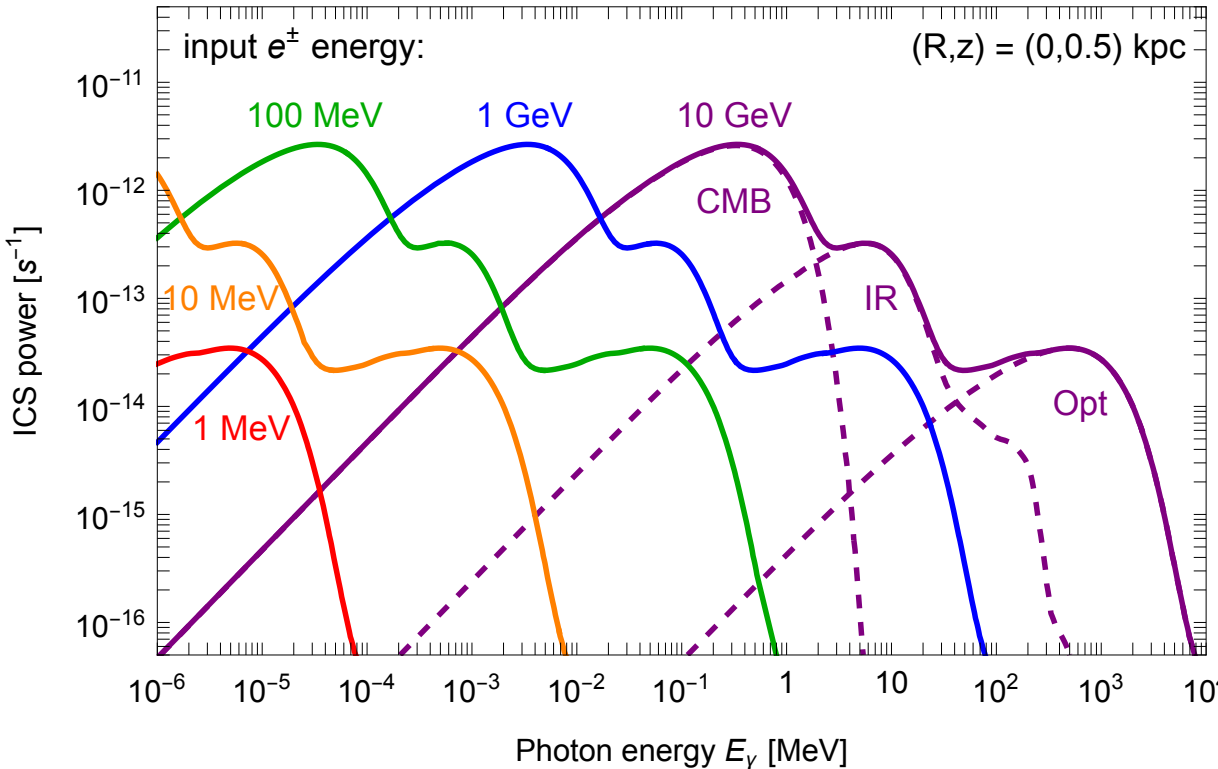
$$y = \frac{E_\gamma}{4\gamma_e^2 E_\gamma^0}, \quad \gamma_e = \frac{E_e}{m_e}$$

Inverse-Compton scattering

- To compute the IC-scattered photon flux, we need a few ingredients:



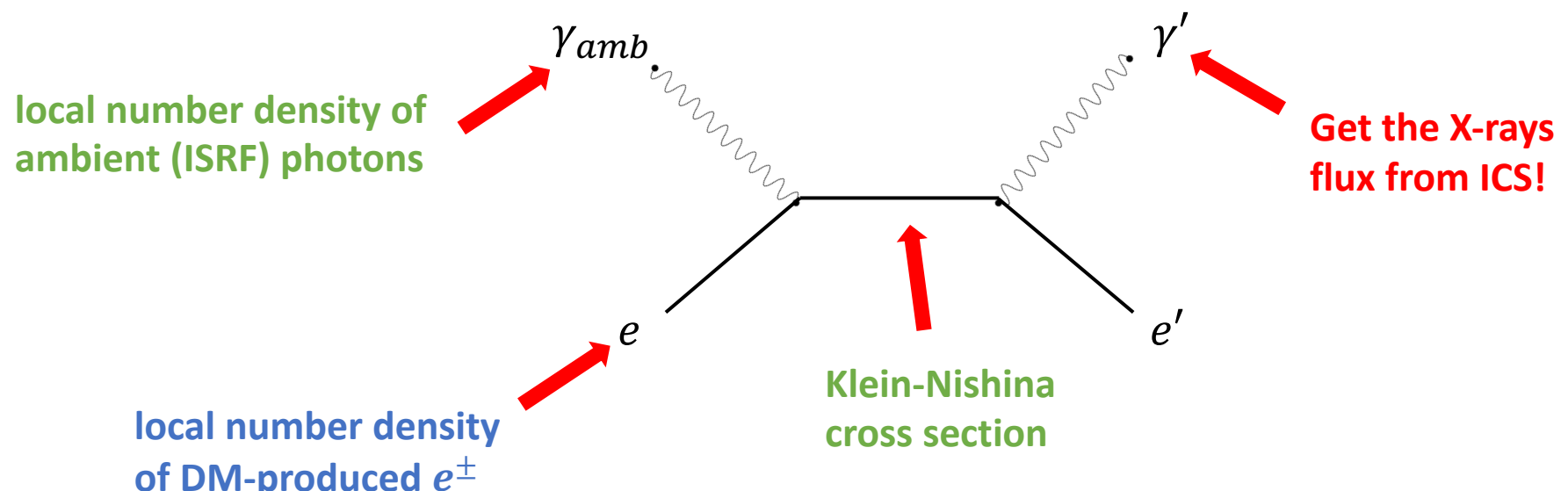
Inverse-Compton scattering



$$\mathcal{P}_{IC,i}(E_\gamma, E_e, \vec{x}) = E_\gamma \int dy n_i(y, \vec{x}) \sigma_{IC}(E_e, y)$$

Inverse-Compton scattering

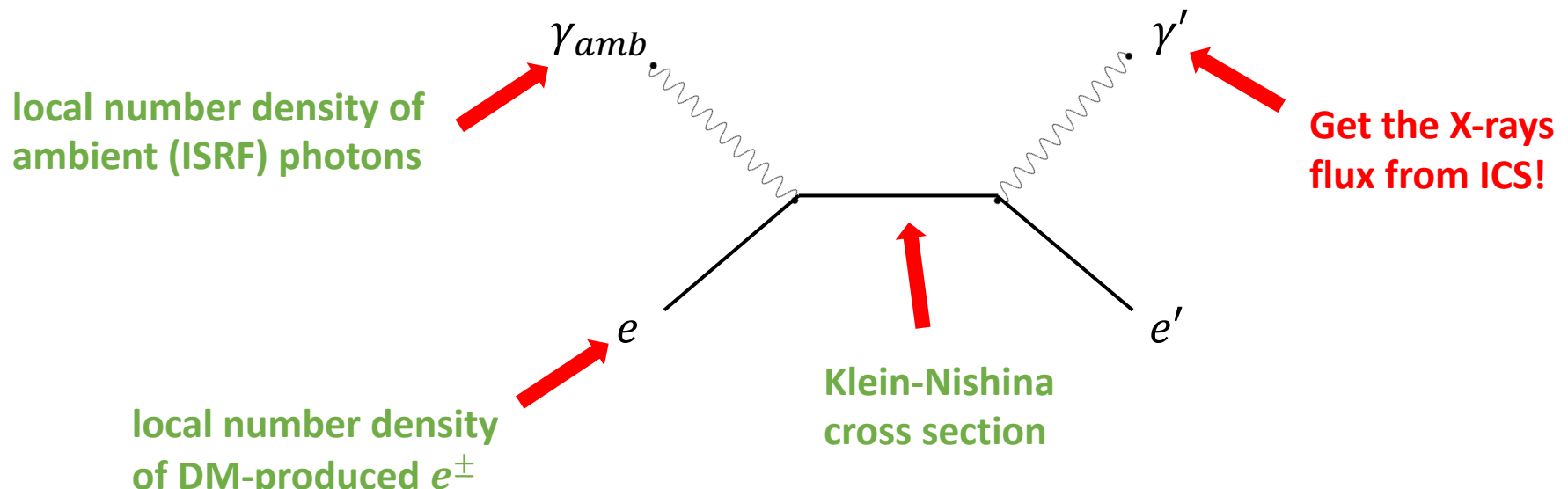
- To compute the IC-scattered photon flux, we need a few ingredients:



$$j(E_\gamma, \vec{x}) = 2 \int_{m_e}^{m_{DM}} dE_e \mathcal{P}_{IC,tot}(E_\gamma, E_e, \vec{x}) f(E_e, \vec{x})$$

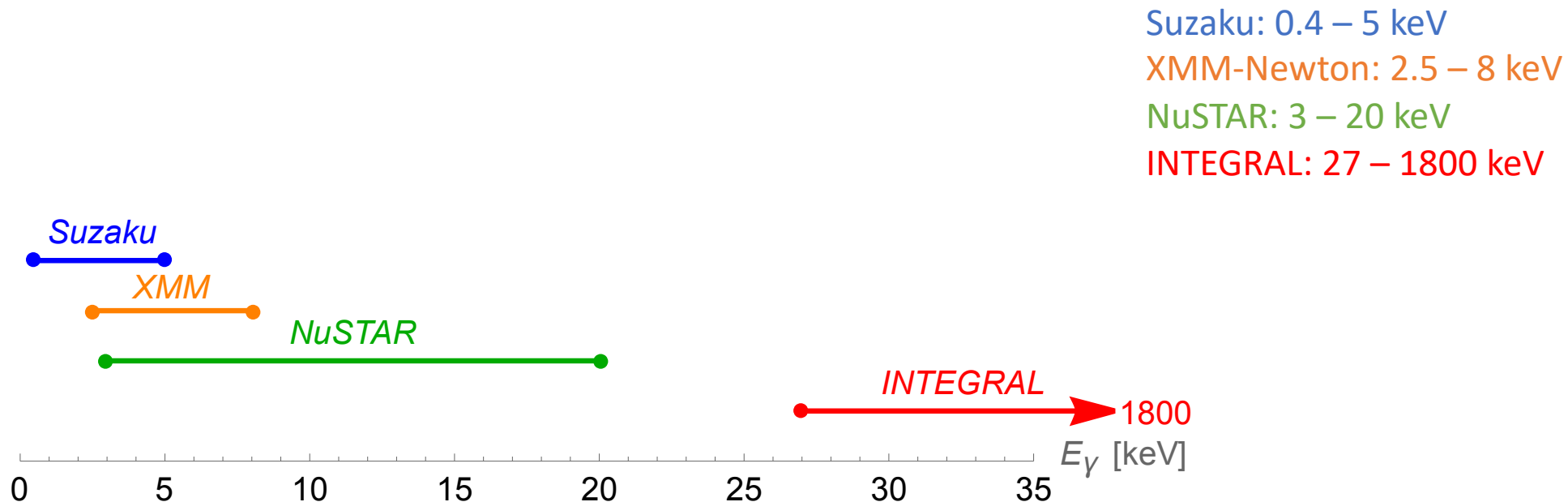
Inverse-Compton scattering

- To compute the IC-scattered photon flux, we need a few ingredients:

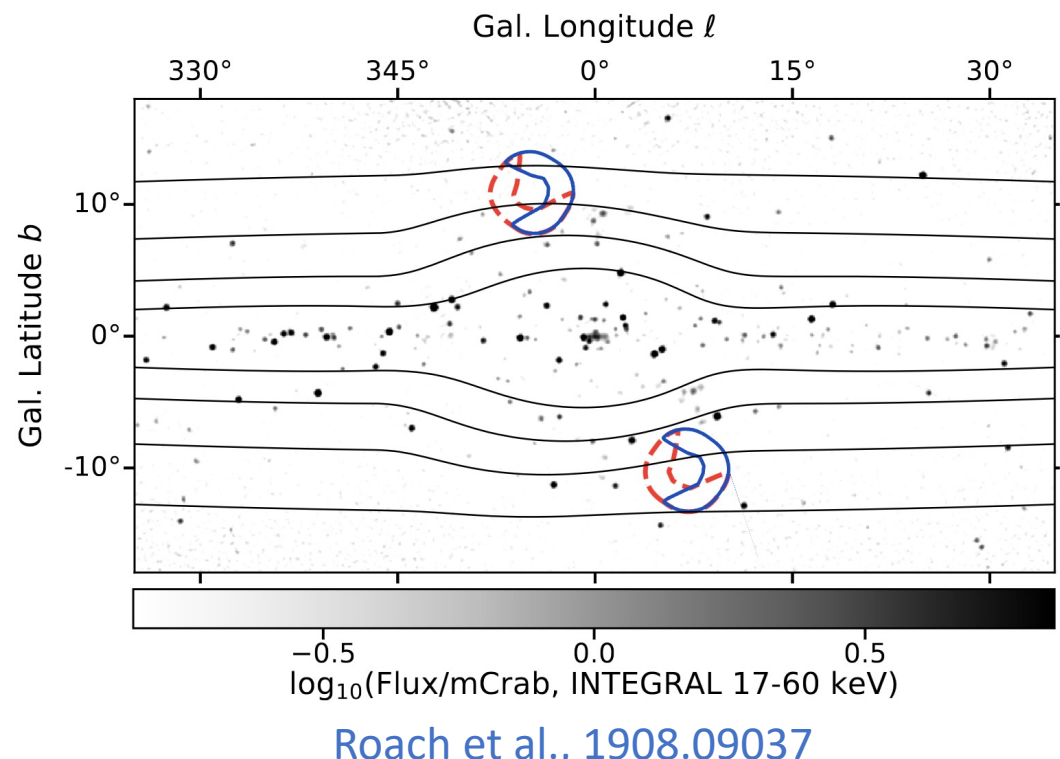
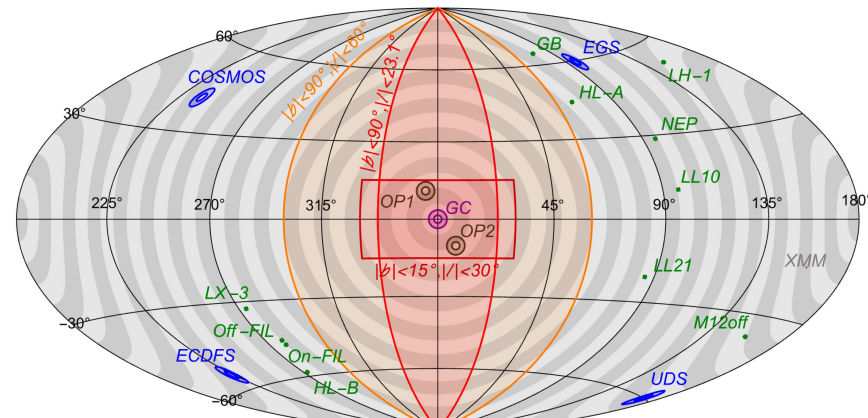
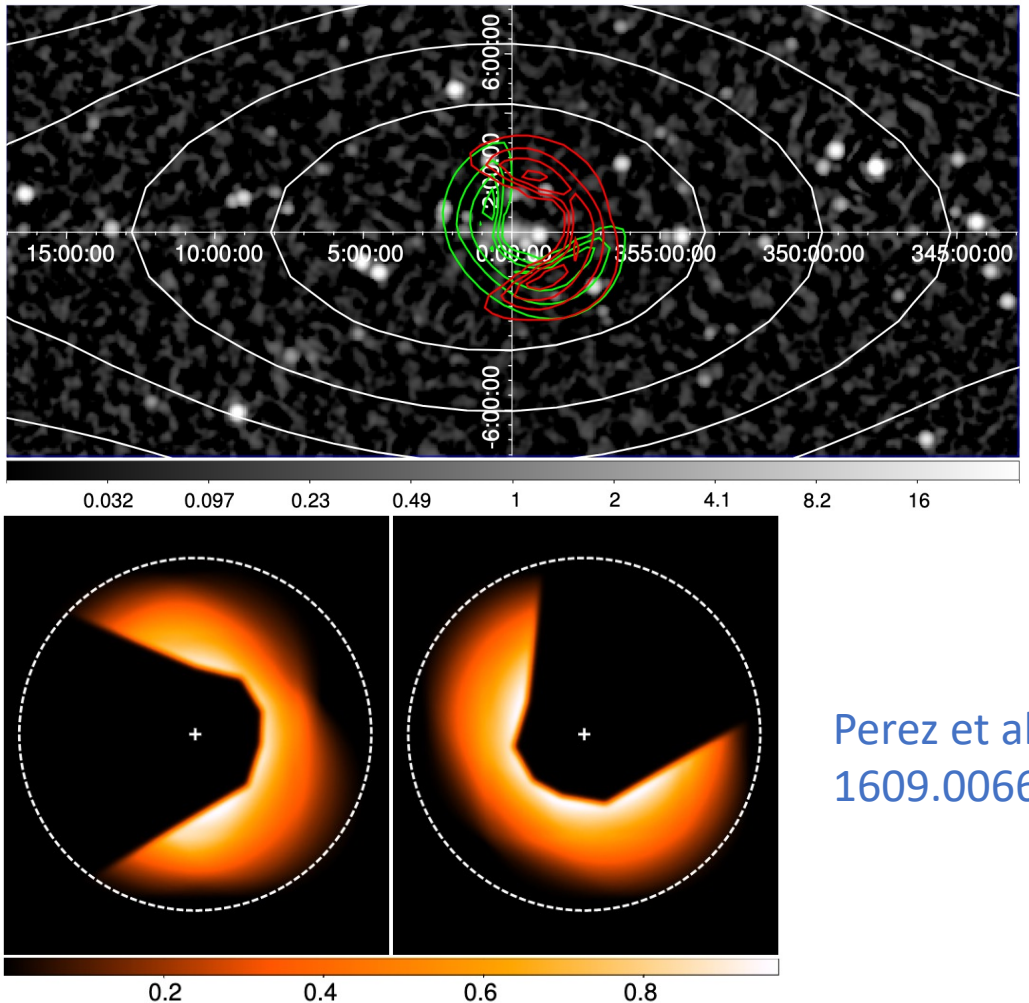


$$\frac{d\Phi_{IC\gamma}}{dE_\gamma d\Omega} = \frac{1}{4\pi E_\gamma} \int_{l.o.s.} ds j(E_\gamma, \vec{x}(s, b, l))$$

Dataset energy ranges



NuSTAR datasets



NuSTAR datasets

Table 2. Data sets used in the analysis.

| ID | Field | Begin | End | T_{exp} |
|----|------------|------------|------------|------------------|
| 1 | COSMOS EP1 | 26-12-2012 | 20-01-2013 | 750 ks |
| 2 | COSMOS EP2 | 03-04-2013 | 21-05-2013 | 630 ks |
| 3 | COSMOS EP3 | 03-12-2013 | 25-02-2014 | 1020 ks |
| 4 | EGS | 15-11-2013 | 27-11-2014 | 1.5 Ms |
| 5 | ECDFS | 28-09-2012 | 01-04-2013 | 1.4 Ms |
| 6 | UDS | 24-01-2016 | 18-11-2016 | 1.7 Ms |

Krionos et al., 2011.11469

Data taken between 2012 and 2016

TABLE I. *NuSTAR* observations used for this analysis.

| Observation ID | Pointing (J2000) ^a RA (deg) | Pointing (J2000) ^a DEC (deg) | Effective Exposure ^b FPMA / FPMB (ks) | Detector Area ^c FPMA / FPMB (cm ²) | Avg. Solid Angle ^d FPMA / FPMB (deg ²) |
|----------------|---|--|---|--|--|
| 40032001002 | 265.8947 | -29.5664 | 39.7 / 39.6 | 9.89 / 11.10 | 3.73 / 4.09 |
| 40032002001 | 265.7969 | -29.5139 | 39.8 / 39.6 | 7.14 / 8.05 | 4.06 / 4.12 |
| 40032003001 | 265.6991 | -29.4613 | 39.8 / 39.6 | 8.18 / 8.92 | 3.47 / 4.01 |
| 40032004002 | 265.9550 | -29.4812 | 22.6 / 22.7 | 4.19 / 6.54 | 2.34 / 3.13 |
| 40032005002 | 265.8572 | -29.4288 | 25.6 / 25.8 | 9.78 / 7.85 | 3.80 / 3.85 |
| 40032006001 | 265.7595 | -29.3762 | 28.6 / 28.6 | 9.98 / 6.18 | 3.76 / 3.74 |

^a Roll angle was 332° for all.

^b After all data cleaning.

^c After stray light, ghost ray, and bad pixel removal.

^d Average solid angle of sky from which 0-bounce photons can be detected, after correcting for removal of stray light, ghost rays, and bad pixels, as well as efficiency due to vignetting effects.

Perez et al., 1609.00667
Data taken between 2012 and 2014

TABLE I. NuSTAR Galactic Bulge observations used in this analysis, with 0-bounce effective areas after data cleaning.

| NuSTAR obsID | Pointing (J2000) RA, Dec (deg) | Effective Exposure ^a FPMA / B (ks) | Detector Area A_{0b} ^b FPMA / B (cm ²) | Solid Angle $\Delta\Omega_{0b}$ ^c FPMA / B (deg ²) |
|--------------|-----------------------------------|--|--|--|
| 40410001002 | 253.2508, -26.6472 | 50.0 / 49.8 | 11.97 / 11.88 | 4.36 / 4.62 |
| 40410002002 | 280.3521, -27.6344 | 44.7 / 44.6 | 12.71 / 12.60 | 4.53 / 4.56 |

^a After OPTIMIZED SAA filtering and manual data screening.

^b After bad pixel removal (both obsIDs) and point-source masking (40410001002 only).

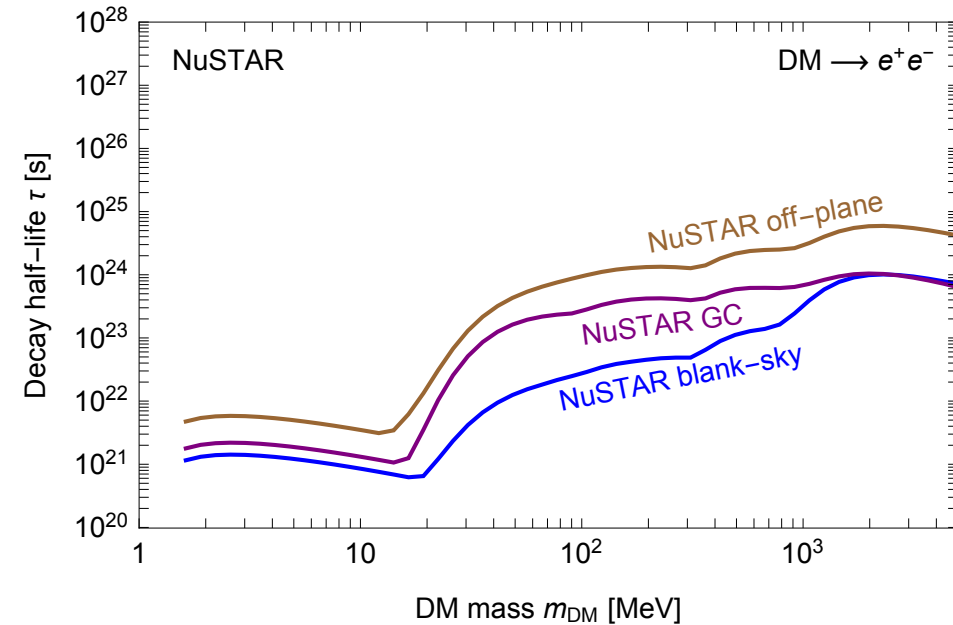
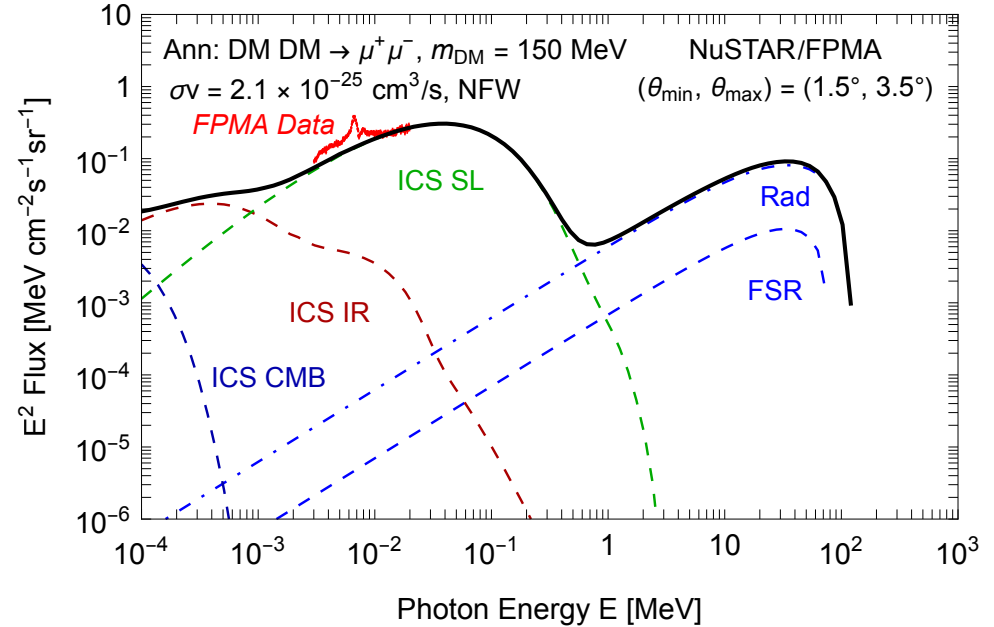
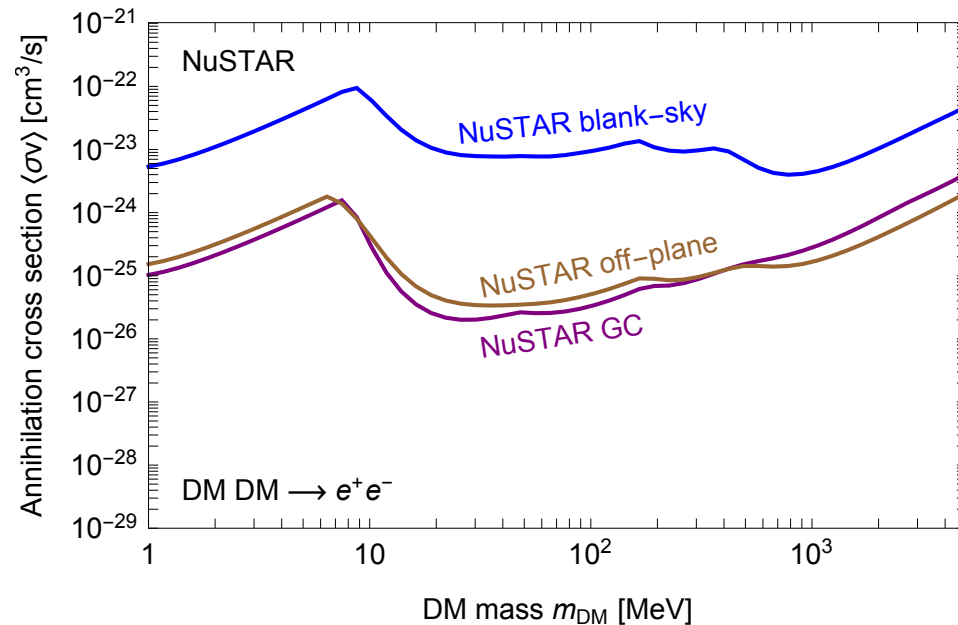
^c Average solid angle of sky for detecting 0-bounce photons, after correcting for bad pixel removal and vignetting efficiency.

Roach et al., 1908.09037
Data taken between in 2018

NuSTAR constraints

NuSTAR (2012-2018 data):

- blank-sky fields [Krivonos et al., 2011.11469](#)
- GC obs. [Perez et al., 1609.00667](#)
- off-plane obs. [Roach et al., 1908.09037](#)



Suzaku datasets

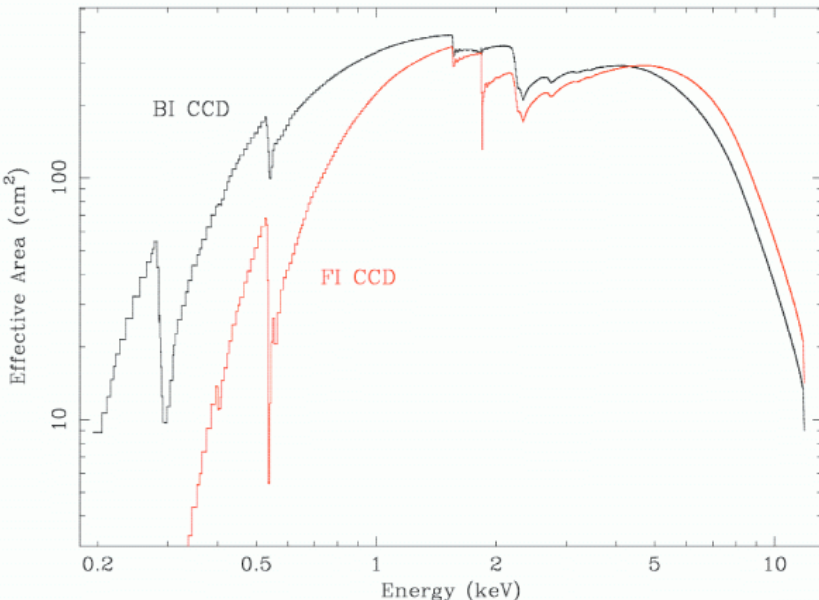
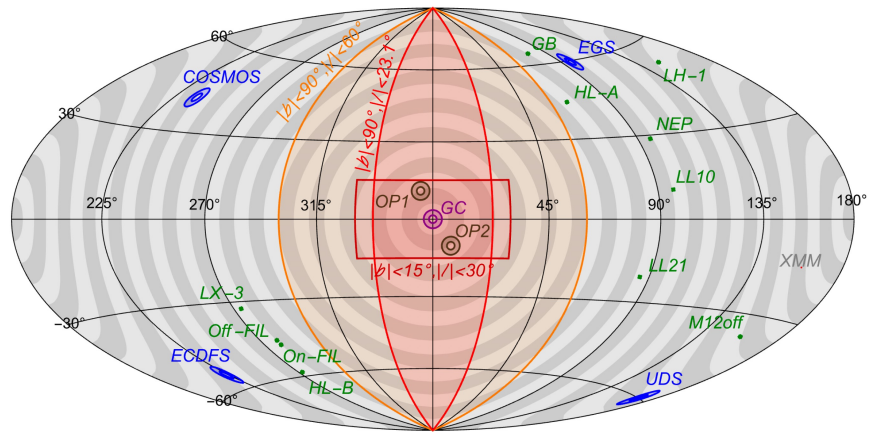
Table 1. Log of observations, ordered by $|b|$

| Data set ID | Field Name (Short Name) | Obs ID | Date | Exposure (ks) | | Aim point (ℓ, b) ($E_{\text{Lon}}, E_{\text{Lat}}$) [*] |
|-------------|---|-----------|-----------------|---------------|---------|---|
| | | | | Total | Cleaned | |
| 1 | GB1428+4217 (GB) | 701092010 | Jun 12-13, 2006 | 48.7 | 34.9 | (75.9, 64.9) (194.2, 52.7) |
| 2 | High latitude B (HL-B) | 500027020 | Feb 17-20, 2006 | 103.6 | 29.7 | (272.4, -58.3) (4.4, -61.4) |
| 3 | Lockman hole 2 (LH-2) | 101002010 | May 17-19, 2006 | 80.4 | 40.0 | (149.7, 53.2) (137.1, 45.1) |
| 4 | Lockman hole 1 (LH-1) | 100046010 | Nov 14-15, 2005 | 77.0 | 61.7 | (149.0, 53.2) (137.2, 45.5) |
| 5 | Off Filament ^a (Off-FIL) | 501001010 | Mar 1-2, 2006 | 80.1 | 59.6 | (278.7, -47.1) (354.8, -72.6) |
| 6 | On Filament ^a (On-FIL) | 501002010 | Mar 3-6 , 2006 | 101.4 | 59.2 | (278.7 , -45.3) (354.1, -74.4) |
| 7 | High latitude A (HL-A) | 500027010 | Feb 14-15, 2006 | 73.6 | 53.2 | (68.4, 44.4) (228.8, 63.5) |
| 8 | MBM12 off cloud ^{b,e} (M12off) | 501104010 | Feb 6-8, 2006 | 75.3 | 51.0 | (157.3, -36.8) (44.5, 2.3) |
| 9 | LMC X-3 Vicinity ^c (LX-3) | 500031010 | Mar 17-18, 2006 | 82.0 | 56.1 | (273.4, -32.6) (41.2, -86.2) |
| 10 | North Ecliptic Pole 1 ^d (NEP1) | 100018010 | Sep 2-4, 2005 | 106.2 | 58.7 | (95.8, 28.7) (334.8, 88.7) |
| 11 | North Ecliptic Pole 2 (NEP2) | 500026010 | Feb 10-12, 2006 | 75.6 | 16.5 | (95.8, 28.7) (334.8, 88.7) |
| 12 | Low latitude 86-21 (LL21) | 502047010 | May 9-10, 2007 | 81.5 | 57.0 | (86.0, -20.8) (347.6, 38.4) |
| 13 | Low latitude 97+10 (LL10) | 503075010 | Apr 15-16, 2008 | 79.8 | 40.8 | (96.6, 10.4) (0.7, 70.6) |
| R1 | MBM12 on cloud ^{b,e} (M12on) | 500015010 | Feb 3-6, 2006 | 102.9 | 68.0 | (159.2, -34.5) (47.2, 2.6) |
| R2 | Midplane 235 ^e (MP235) | 502021010 | Apr 22-25, 2007 | 189.5 | 53.0 | (235.0, 0.0) (119.5, -40.6) |

Results previously published by ^a Henley et al. (2007), ^b Smith et al. (2007), ^c Yao et al. (2009), ^d Fujimoto et al. (2007), ^e Masui et al. (2009).

* Ecliptic coordinate

Yoshino et al., 0903.2981

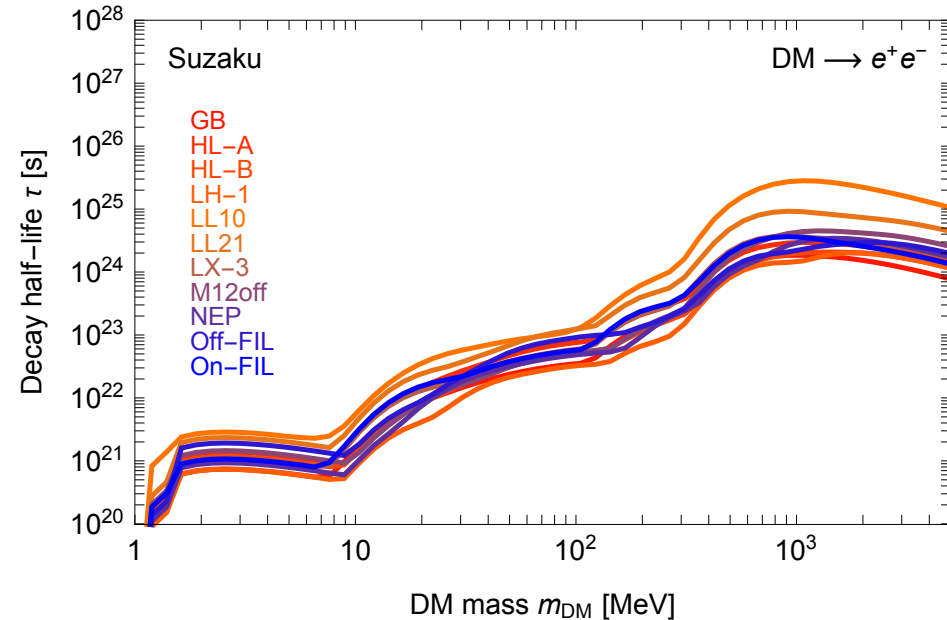
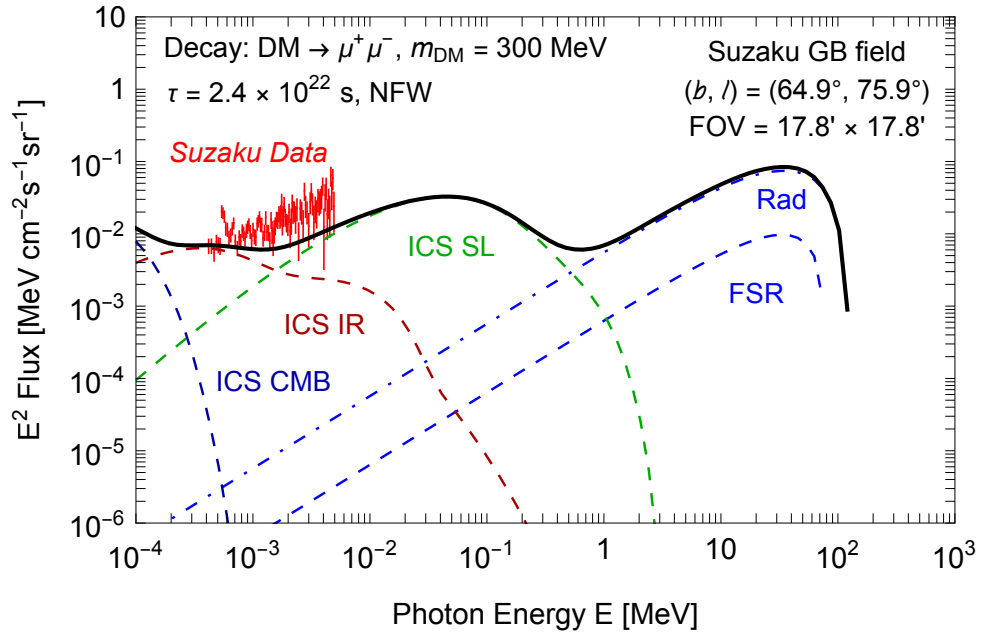
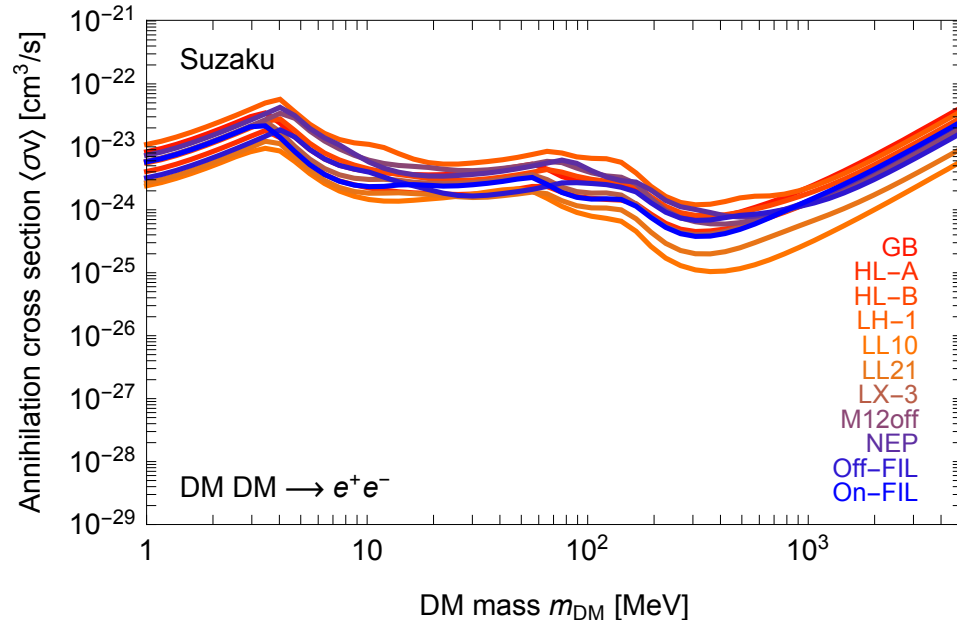


https://heasarc.gsfc.nasa.gov/docs/suzaku/gallery/performance/xis_area.html

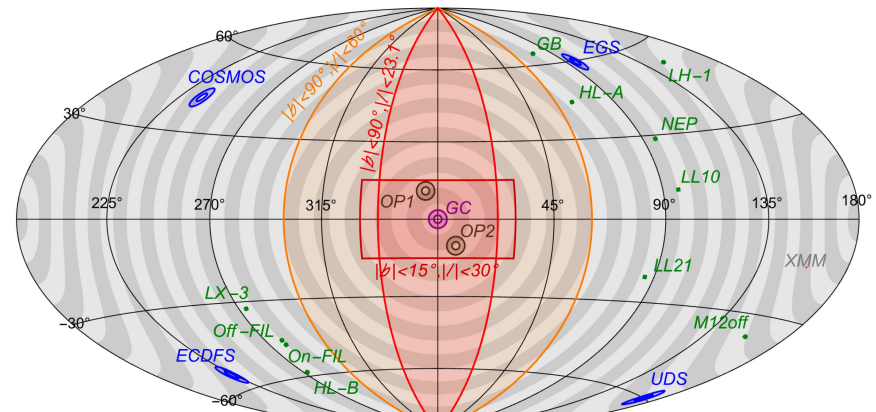
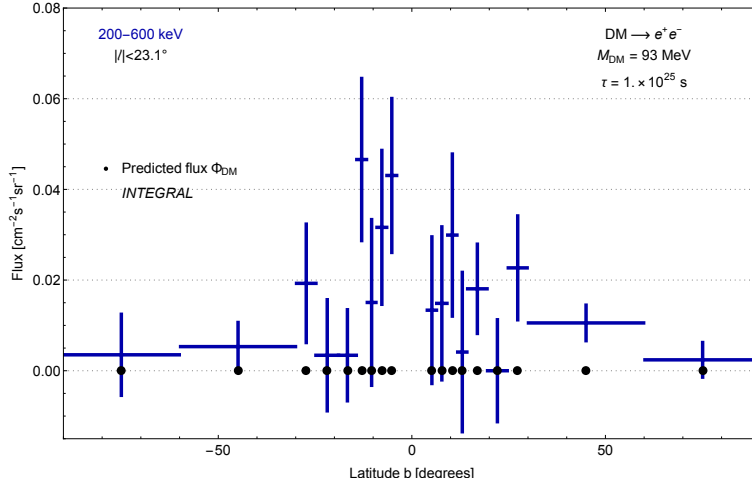
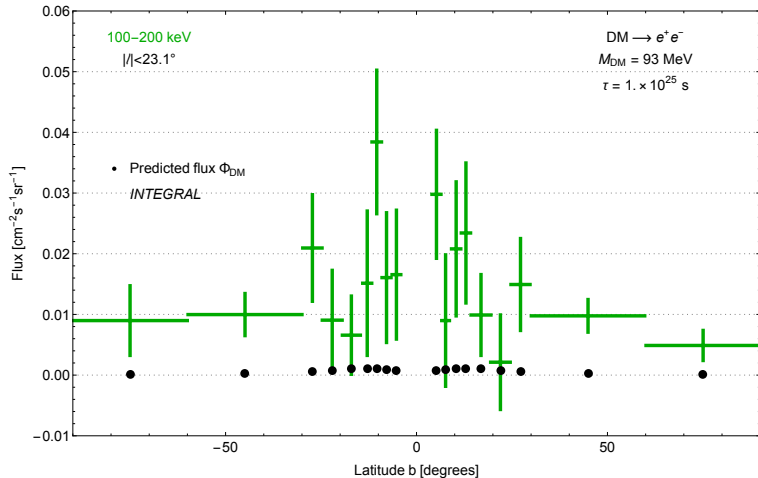
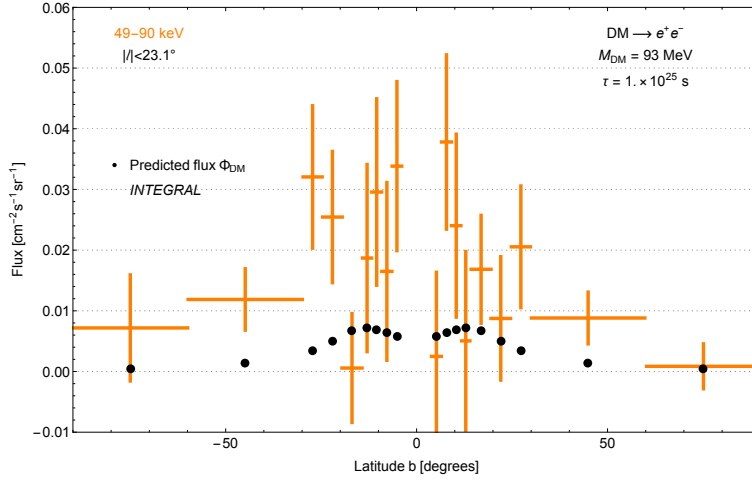
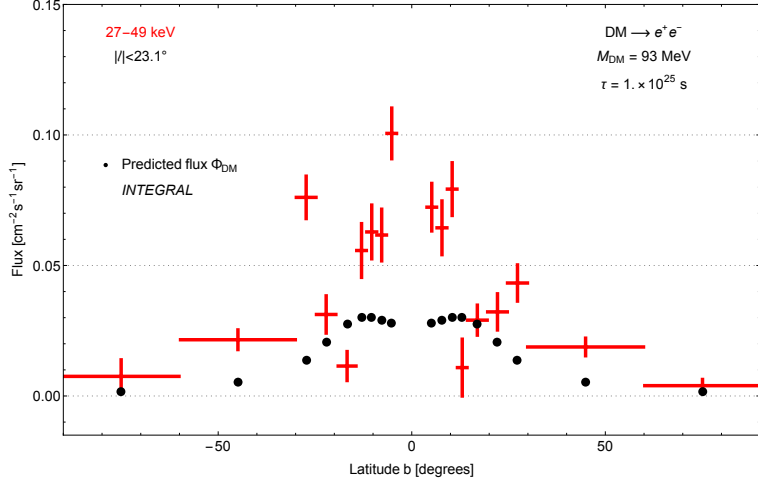
Suzaku constraints

Suzaku high-latitude fields
2006-2008

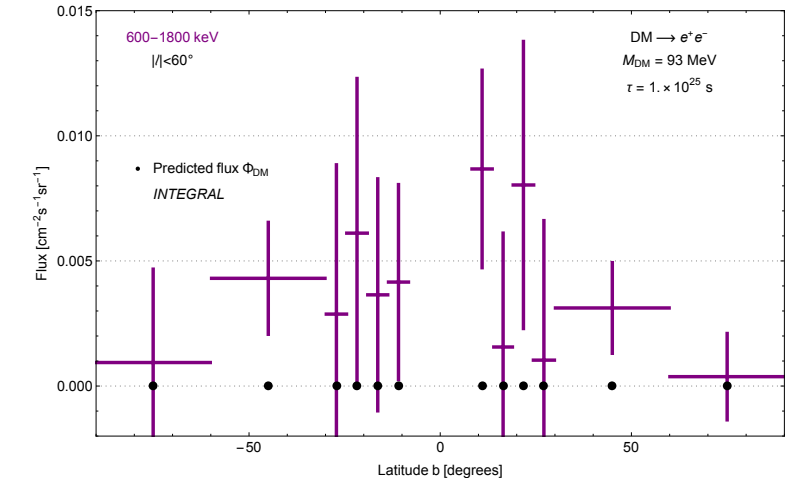
[Yoshino et al., 0903.2981](#)



INTEGRAL datasets



Bouchet et al., INTEGRAL coll.,
1107.0200

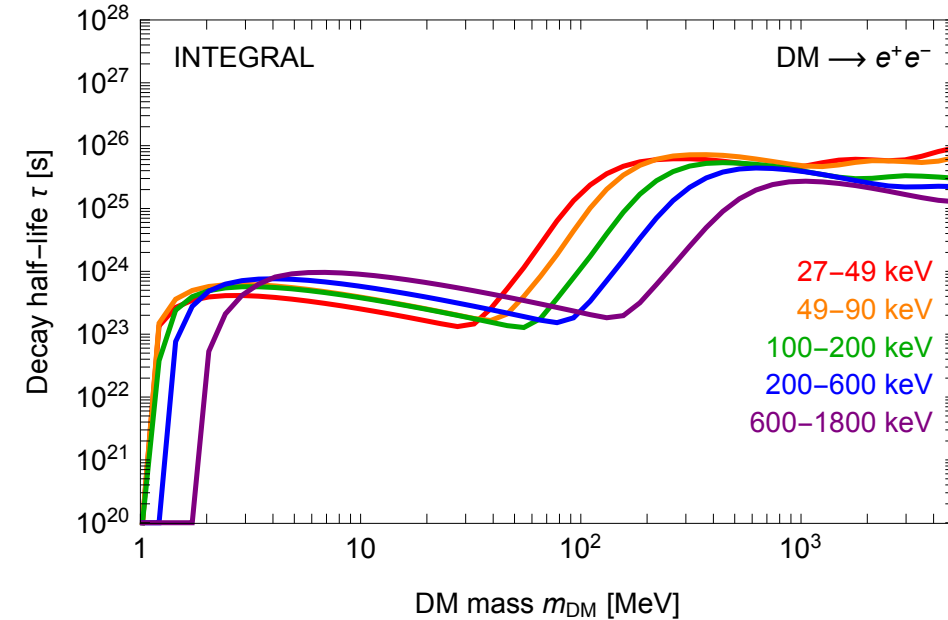
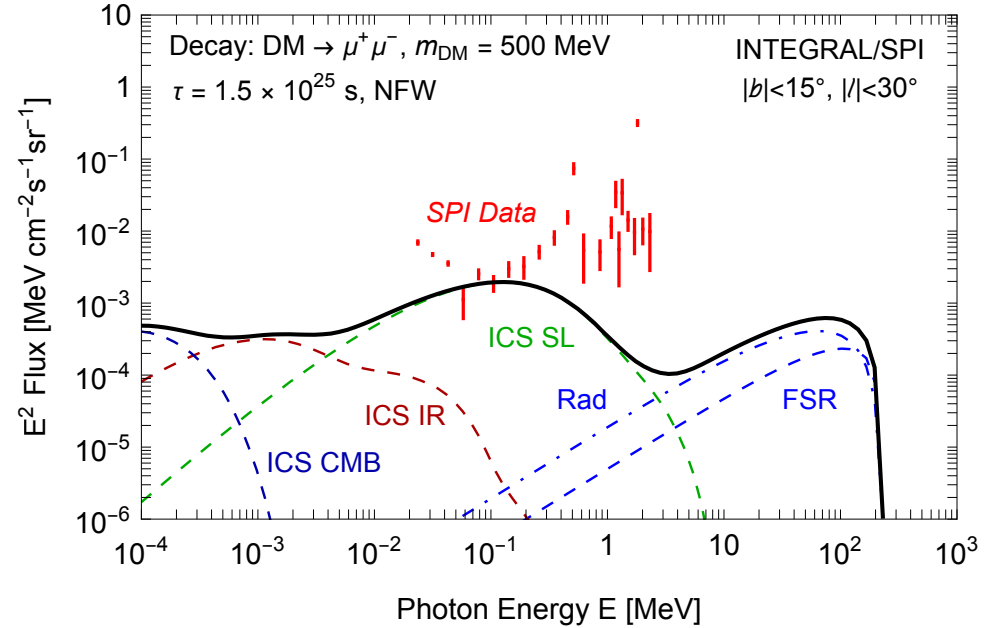
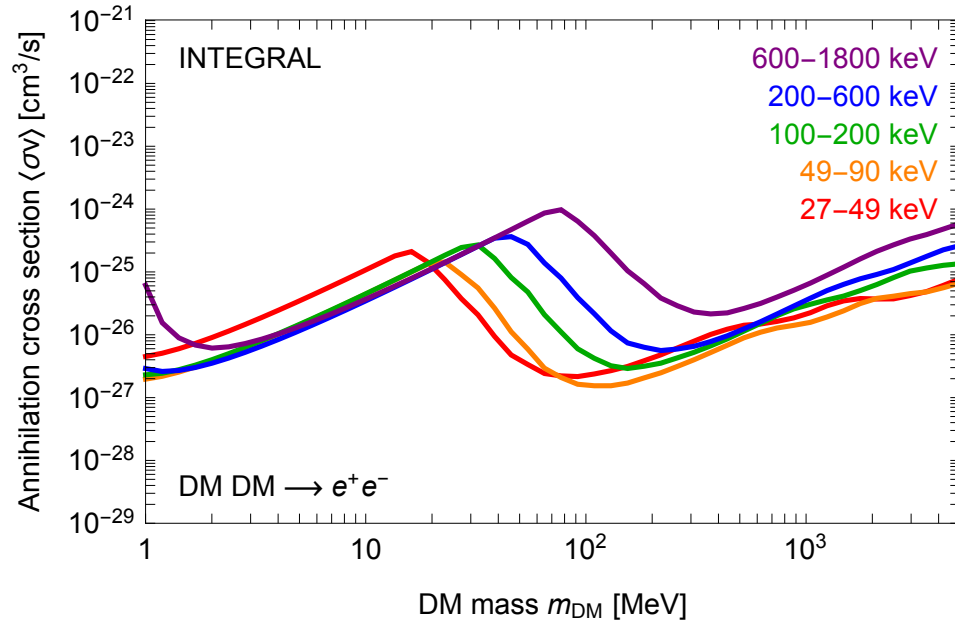


INTEGRAL constraints

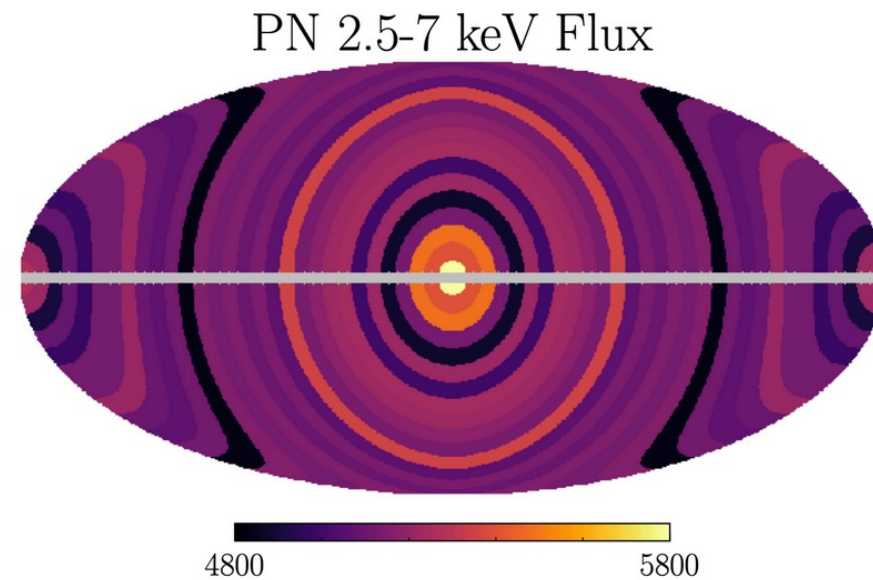
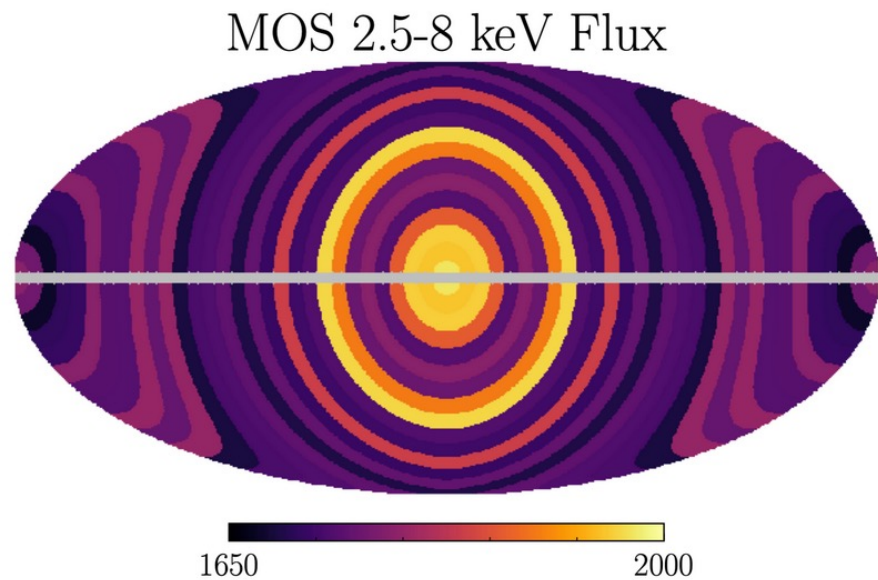
INTEGRAL diffuse emission searches

2003-2009

Bouchet et al., INTEGRAL coll., 1107.0200



XMM-Newton datasets



https://github.com/bsafdi/XMM_BSO_DATA

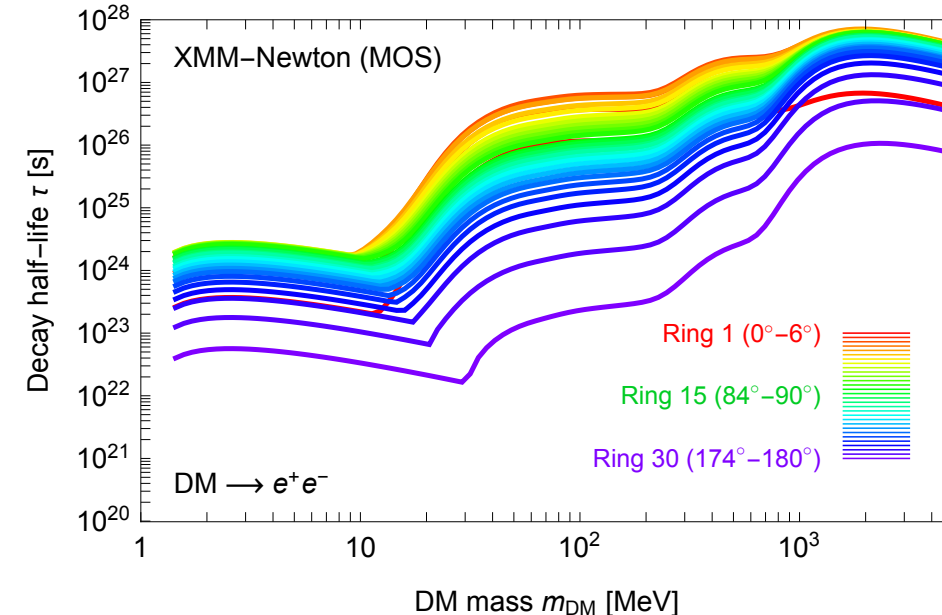
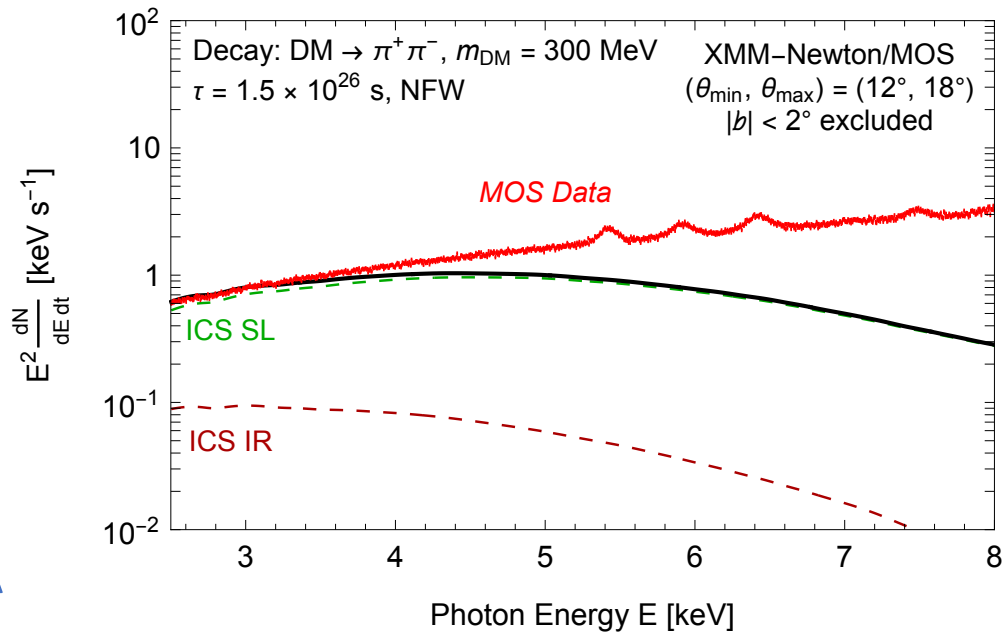
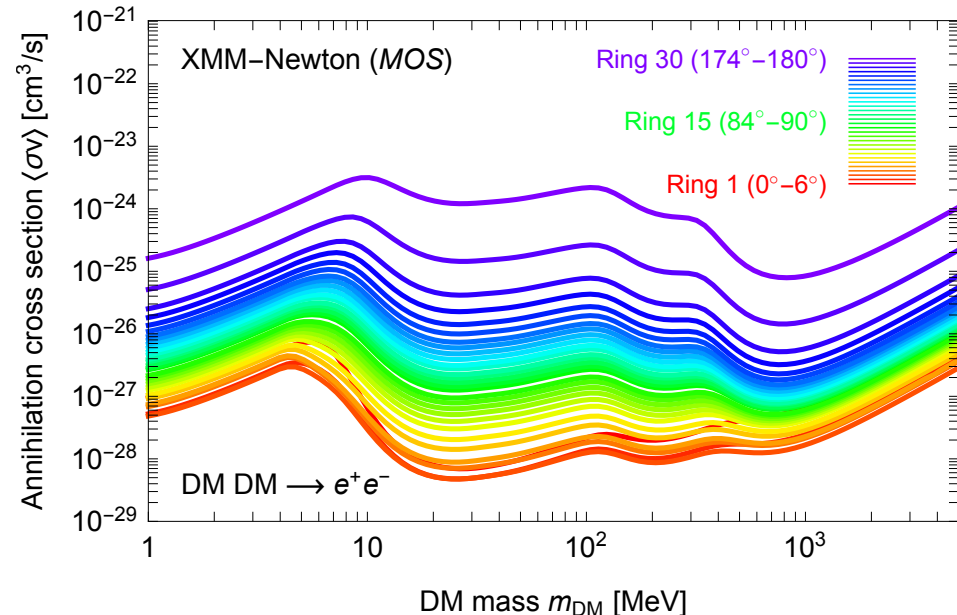
Datasets + Instrument response functions

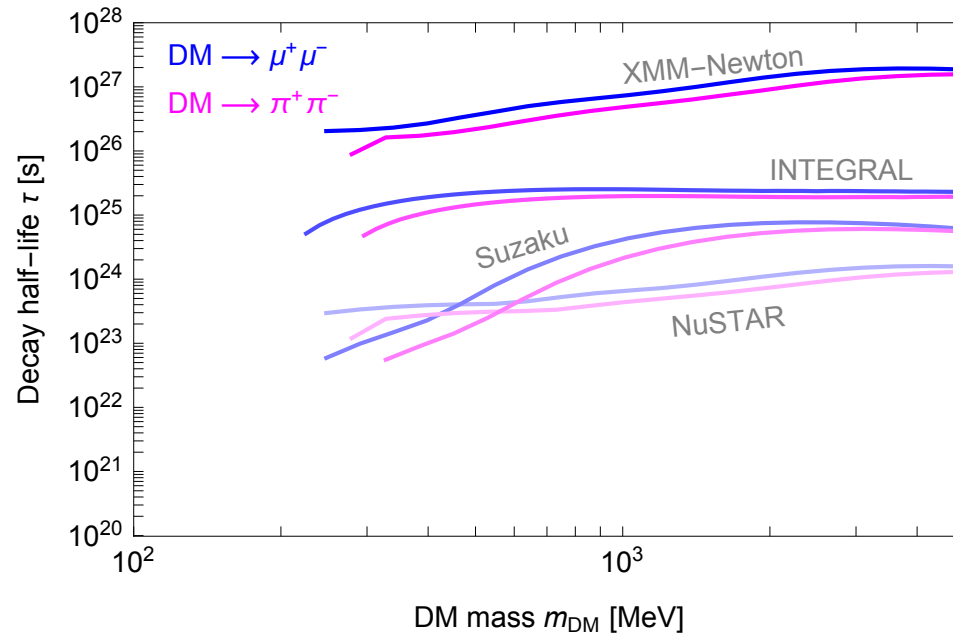
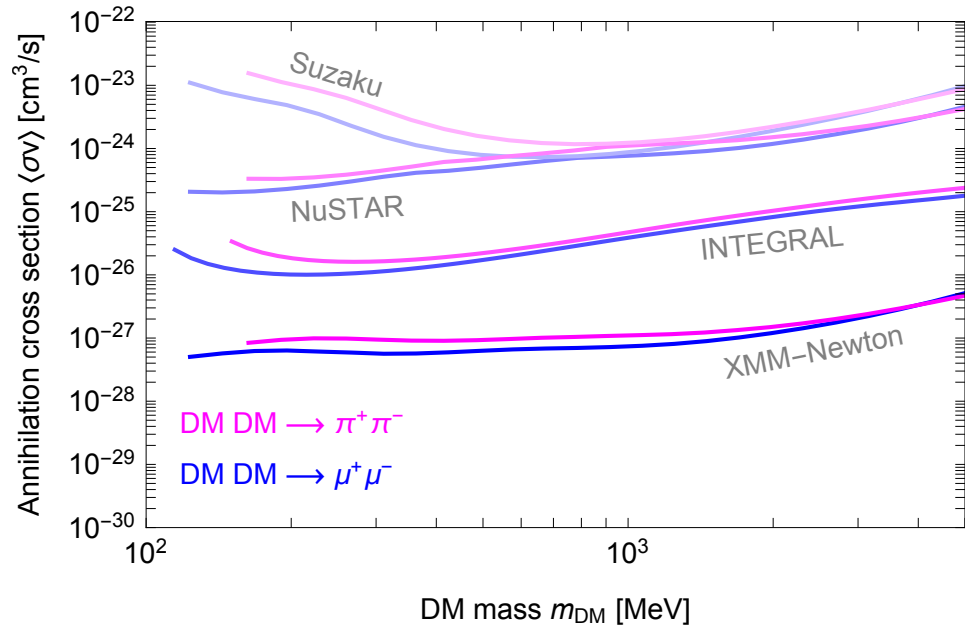
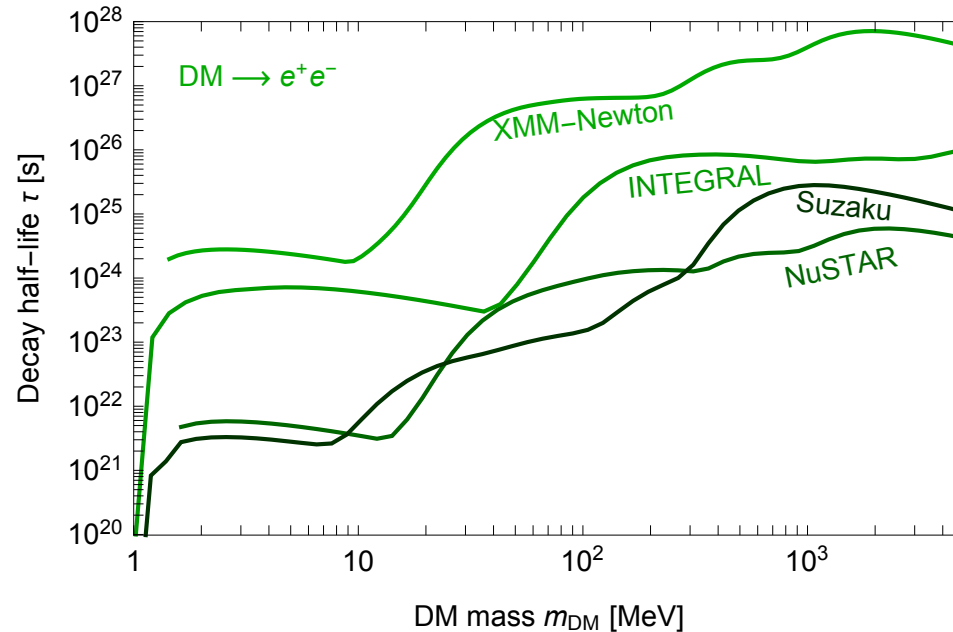
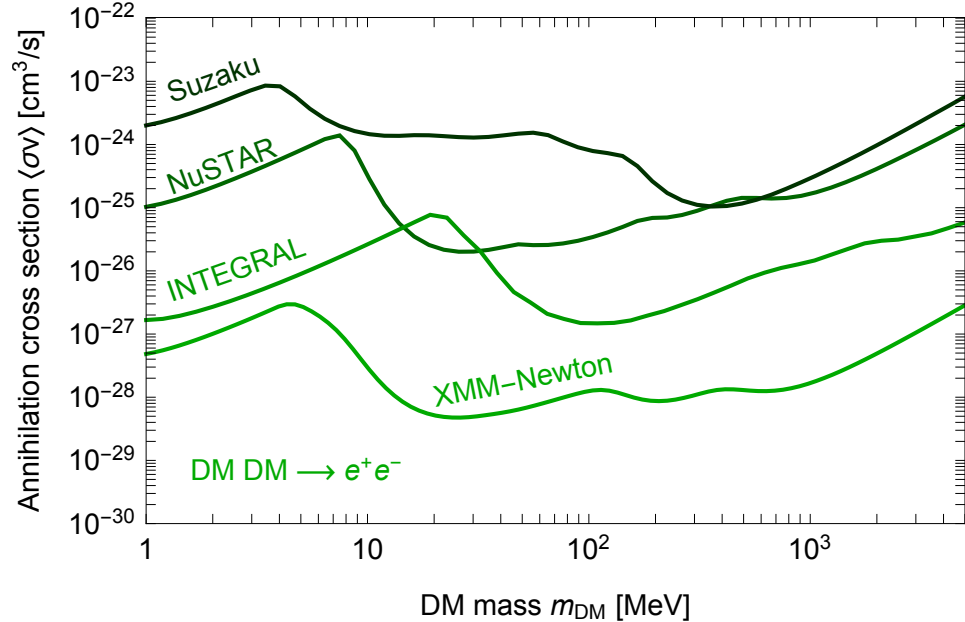
XMM-Newton constraints

XMM-Newton whole-sky observations
1999-2018

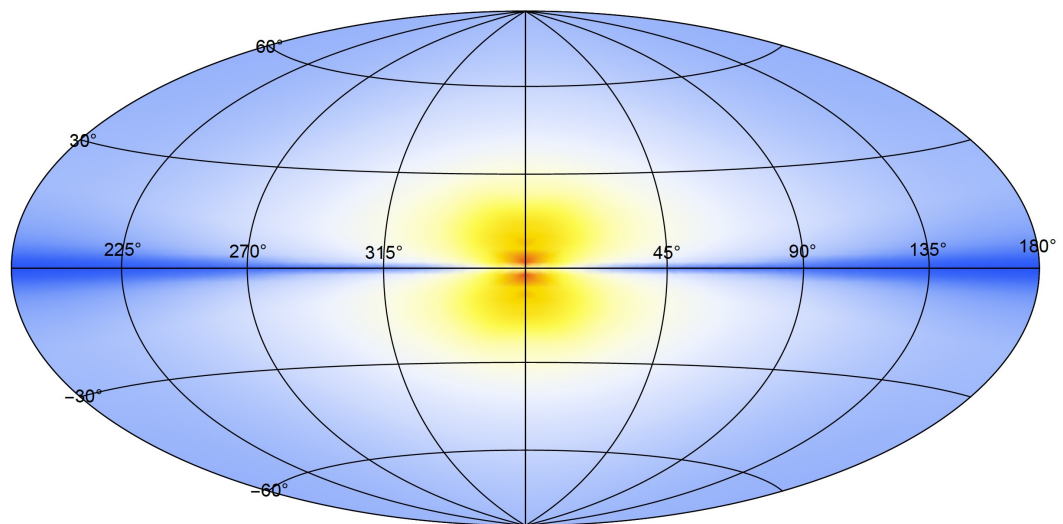
Foster et al., 2102.02207

https://github.com/bsafdi/XMM_BSO_DATA

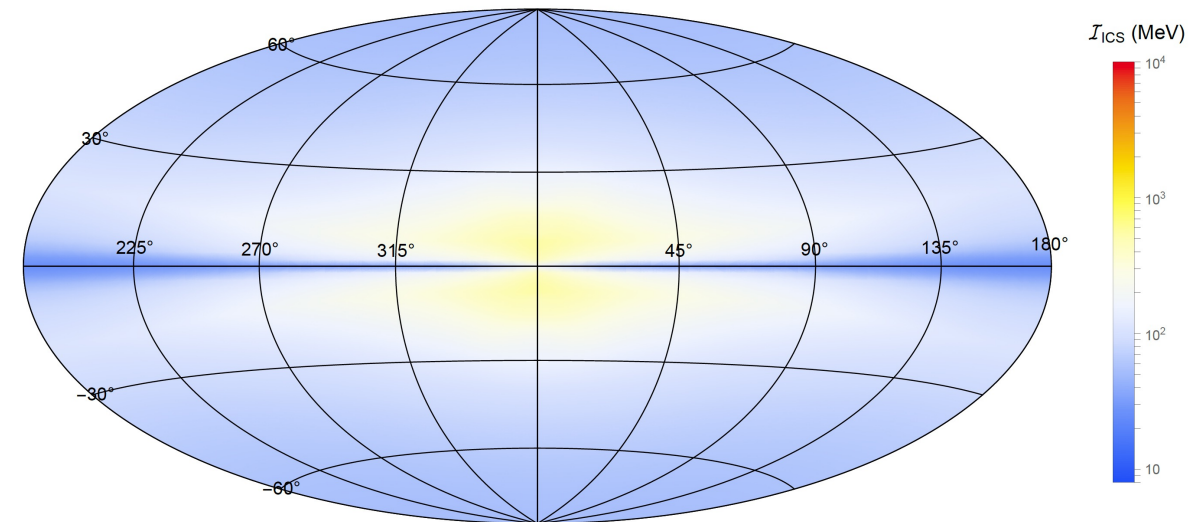
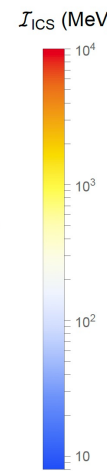




ICS halo function (spatial distribution)



Annihilation ($\eta = 2$)

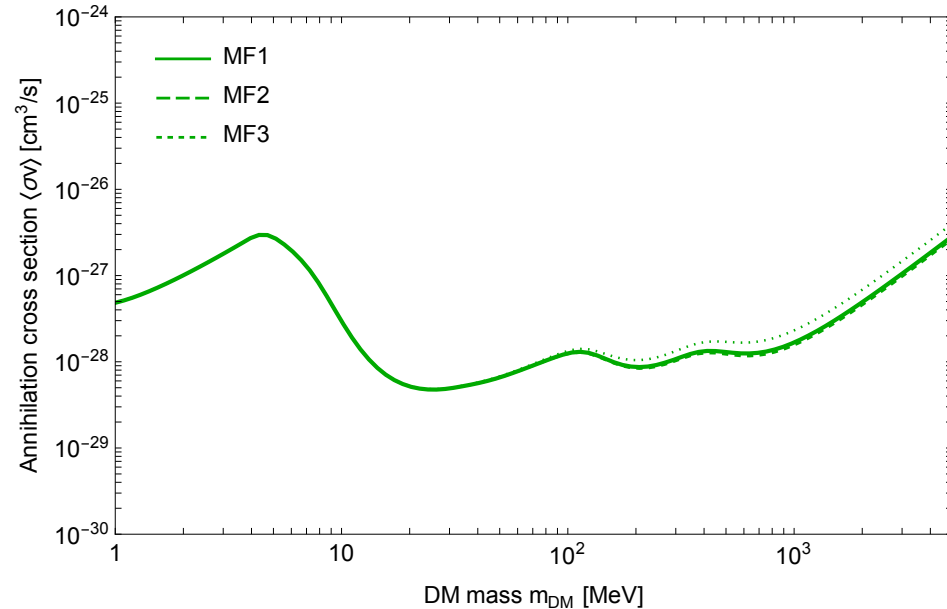
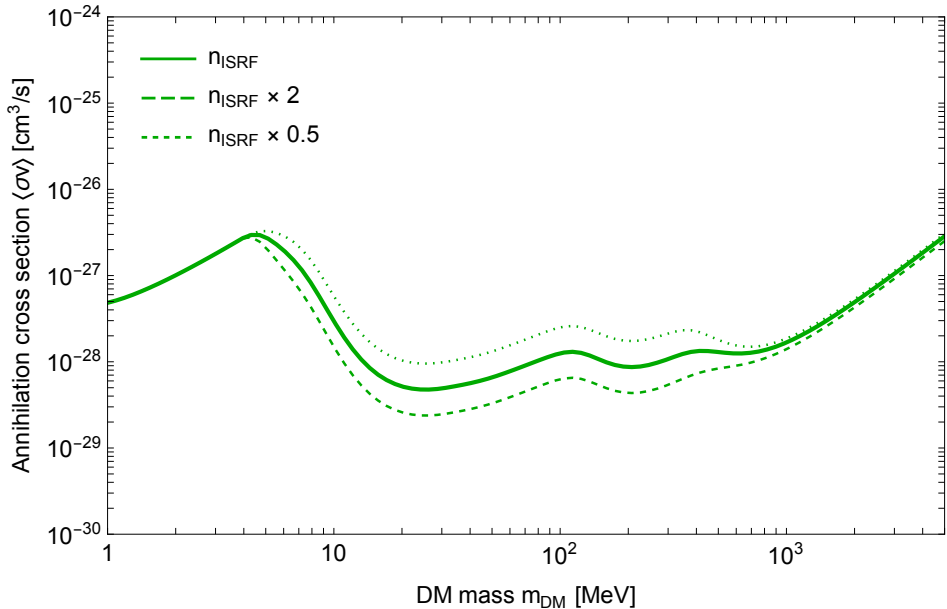
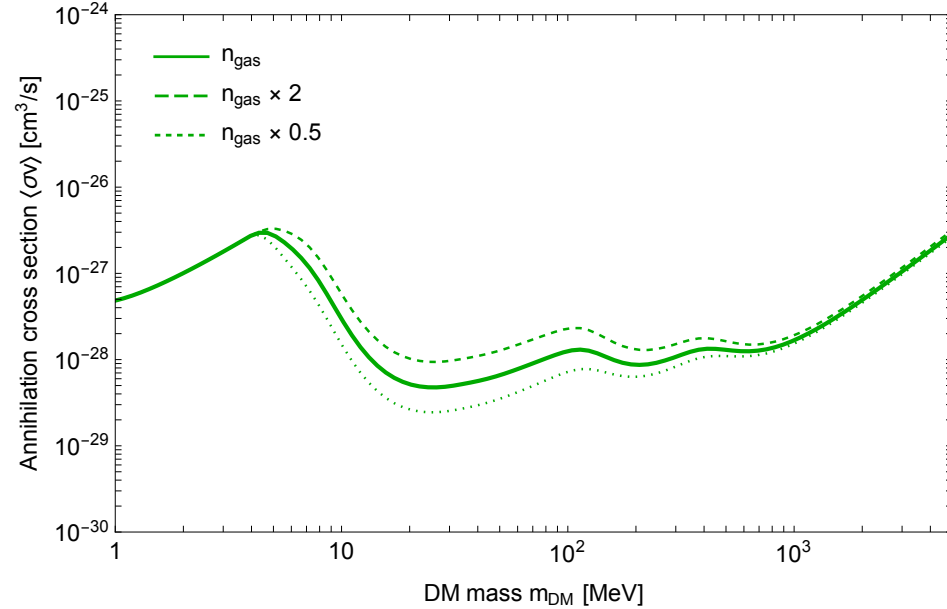
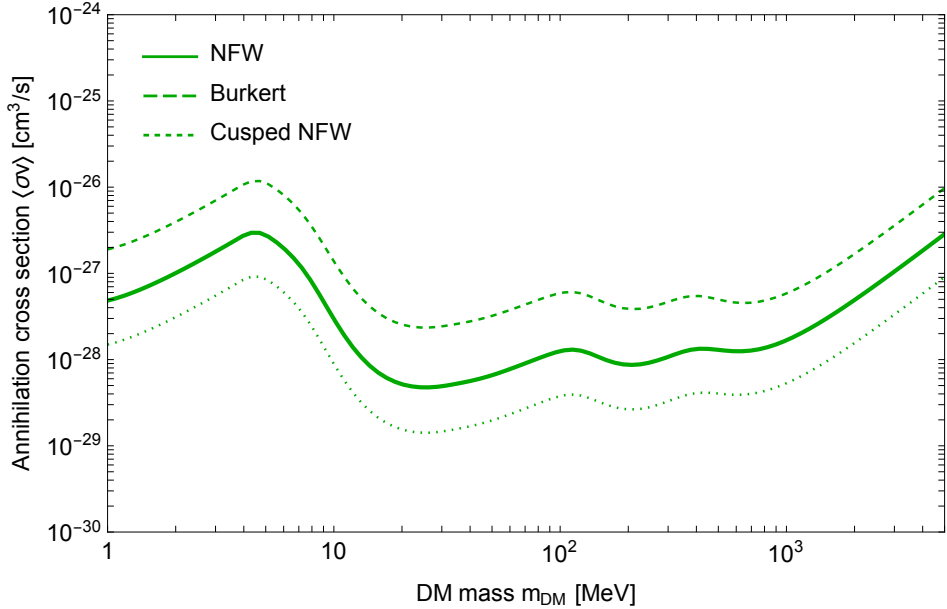


Decay ($\eta = 1$)

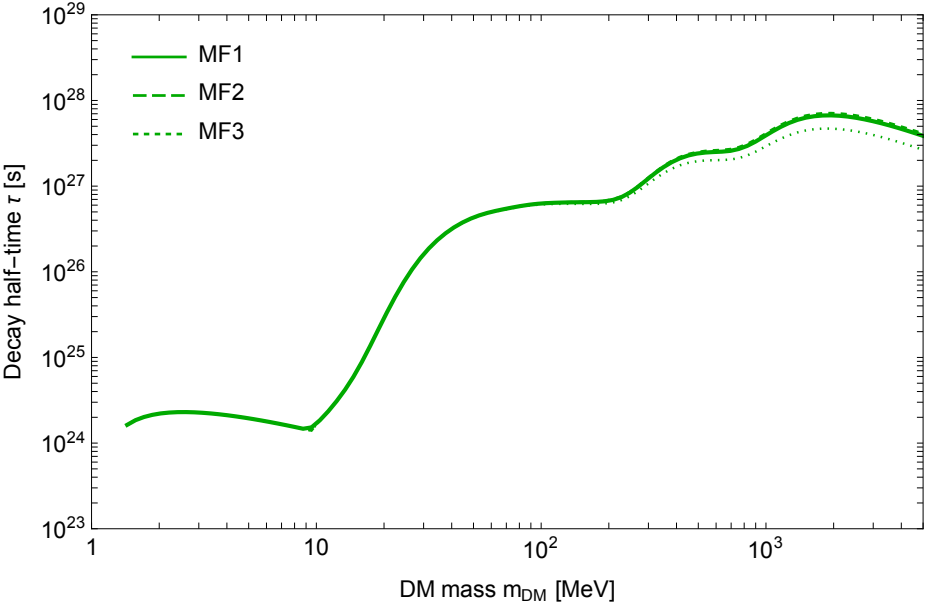
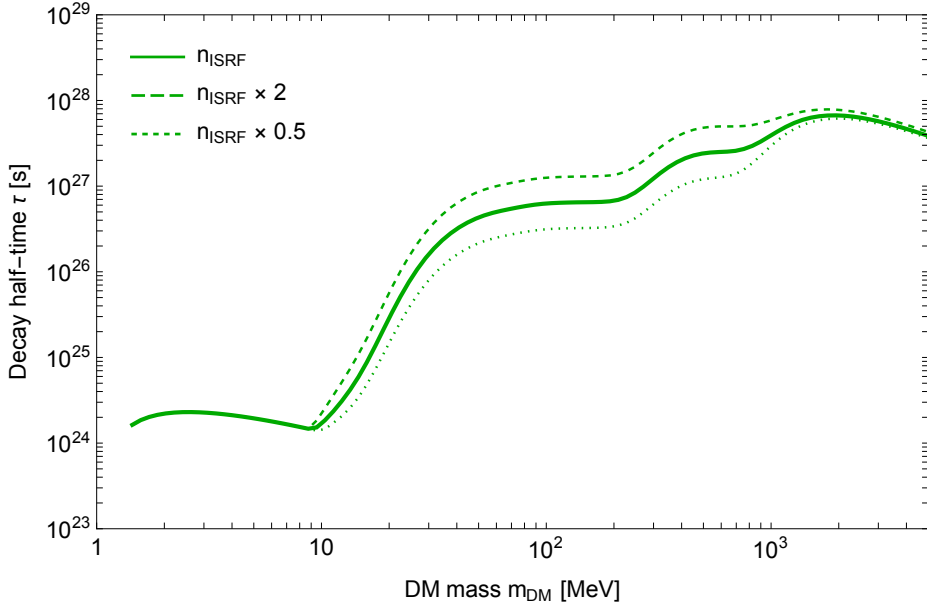
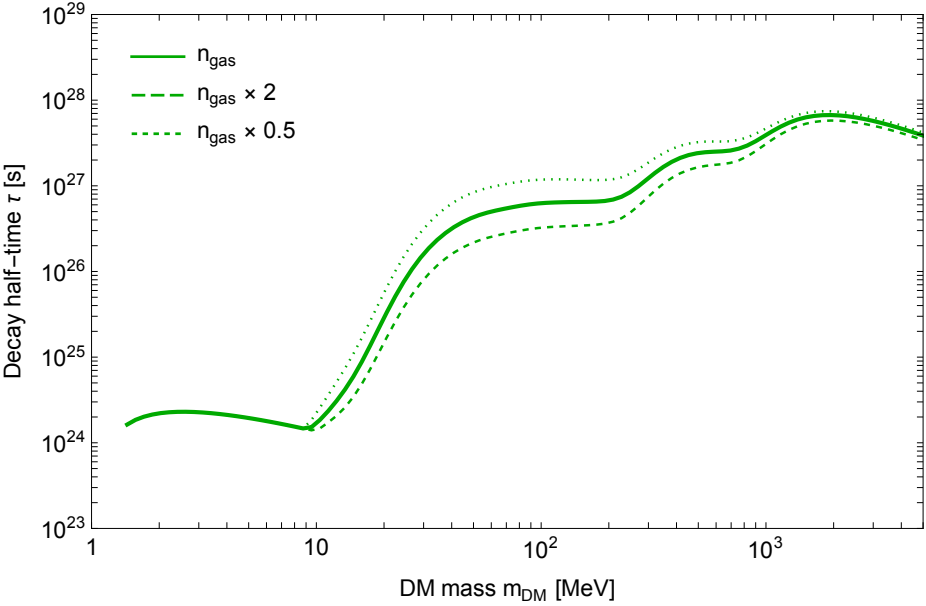
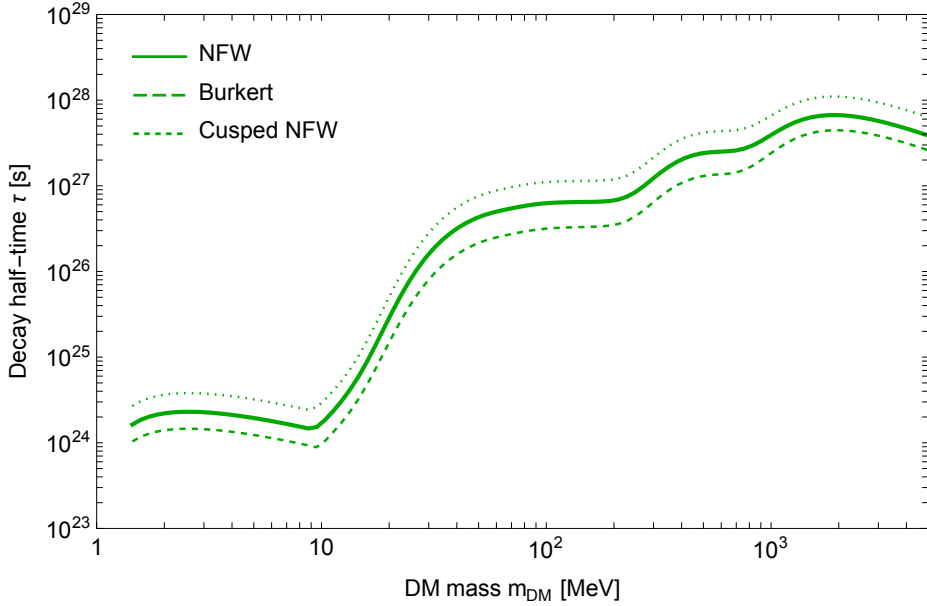
$$I_{\text{ICS}}(E_\gamma, E_e, b, l) = 2 E_\gamma \int_{l.o.s.} \frac{ds}{r_\odot} \left(\frac{\rho(s, b, l)}{\rho_\odot} \right)^\eta \int_{m_e}^{E_e} dE \frac{\mathcal{P}_{\text{IC}}(E_\gamma, E, s, b, l)}{b(E, s, b, l)}$$

$$\begin{aligned} E_\gamma &= 5 \text{ keV} \\ E_e &= 1 \text{ GeV} \end{aligned}$$

$\text{DM DM} \rightarrow e^+ e^-$



$\text{DM} \rightarrow e^+ e^-$



Galactic magnetic field configurations

$$B(r, z) = B_0 \exp\left(-\frac{r - r_\odot}{R_D} - \frac{|z|}{z_D}\right)$$

| Models | B_0 (μG) | r_D (kpc) | z_D (kpc) |
|--------|-------------------|-----------------|-----------------|
| MF1 | 4.78 | 10 | 2 |
| MF2 | 5.1 | 8.5 | 1 |
| MF3 | 9.1 | 30 | 4 |